Accurate calculation and modeling of the adiabatic connection in density functional theory

A. M. Teale, S. Coriani, and T. Helgaker

Citation: The Journal of Chemical Physics **132**, 164115 (2010); doi: 10.1063/1.3380834
View online: http://dx.doi.org/10.1063/1.3380834
View Table of Contents: http://scitation.aip.org/content/aip/journal/jcp/132/16?ver=pdfcov
Published by the AIP Publishing

Accurate calculation and modeling of the adiabatic connection in density functional theory

A. M. Teale,[1,a)] S. Coriani,[1,2] and T. Helgaker[1]
[1]*Department of Chemistry, Centre for Theoretical and Computational Chemistry, University of Oslo, P.O. Box 1033, Blindern, Oslo N-0315, Norway*
[2]*Dipartimento di Scienze Chimiche, Università degli Studi di Trieste, Via Licio Giorgieri 1, Trieste I-34127, Italy*

(Received 13 January 2010; accepted 14 March 2010; published online 29 April 2010)

Using a recently implemented technique for the calculation of the adiabatic connection (AC) of density functional theory (DFT) based on Lieb maximization with respect to the external potential, the AC is studied for atoms and molecules containing up to ten electrons: the helium isoelectronic series, the hydrogen molecule, the beryllium isoelectronic series, the neon atom, and the water molecule. The calculation of AC curves by Lieb maximization at various levels of electronic-structure theory is discussed. For each system, the AC curve is calculated using Hartree–Fock (HF) theory, second-order Møller–Plesset (MP2) theory, coupled-cluster singles-and-doubles (CCSD) theory, and coupled-cluster singles-doubles-perturbative-triples [CCSD(T)] theory, expanding the molecular orbitals and the effective external potential in large Gaussian basis sets. The HF AC curve includes a small correlation-energy contribution in the context of DFT, arising from orbital relaxation as the electron-electron interaction is switched on under the constraint that the wave function is always a single determinant. The MP2 and CCSD AC curves recover the bulk of the dynamical correlation energy and their shapes can be understood in terms of a simple energy model constructed from a consideration of the doubles-energy expression at different interaction strengths. Differentiation of this energy expression with respect to the interaction strength leads to a simple two-parameter doubles model (AC-D) for the AC integrand (and hence the correlation energy of DFT) as a function of the interaction strength. The structure of the triples-energy contribution is considered in a similar fashion, leading to a quadratic model for the triples correction to the AC curve (AC-T). From a consideration of the structure of a two-level configuration-interaction (CI) energy expression of the hydrogen molecule, a simple two-parameter CI model (AC-CI) is proposed to account for the effects of static correlation on the AC. When parametrized in terms of the same input data, the AC-CI model offers improved performance over the corresponding AC-D model, which is shown to be the lowest-order contribution to the AC-CI model. The utility of the accurately calculated AC curves for the analysis of standard density functionals is demonstrated for the BLYP exchange-correlation functional and the interaction-strength-interpolation (ISI) model AC integrand. From the results of this analysis, we investigate the performance of our proposed two-parameter AC-D and AC-CI models when a simple density functional for the AC at infinite interaction strength is employed in place of information at the fully interacting point. The resulting two-parameter correlation functionals offer a qualitatively correct behavior of the AC integrand with much improved accuracy over previous attempts. The AC integrands in the present work are recommended as a basis for further work, generating functionals that avoid spurious error cancellations between exchange and correlation energies and give good accuracy for the range of densities and types of correlation contained in the systems studied here.
 [doi:10.1063/1.3380834]

I. INTRODUCTION

Recently, there has been a renewed interest in the construction of exchange-correlation (xc) functionals in density functional theory (DFT) by modeling the adiabatic connection (AC),[1–20] originally introduced in the 1970s by Harris,[1] Langreth and Perdew,[2,5] and Gunnarsson and Lundqvist.[3,4] In particular, the density-fixed AC[2–5] provides the link between the Kohn–Sham (KS) noninteracting system ($\lambda=0$) and the physical interacting system ($\lambda=1$) via a series of partially interacting systems, all fixed at the physical density and described by the Hamiltonian $\hat{H}=\hat{T}+\Sigma_i v_\lambda(\mathbf{r}_i)+\hat{W}_\lambda$, where $\hat{T}$ is the kinetic-energy operator, v_λ the external potential determined so as to keep ρ fixed at the physical density, $\hat{W}_\lambda$ the two-electron interaction operator, and λ the coupling constant, which regulates the strength of the electron-electron interaction. From the concavity of the universal density functional $F_\lambda[\rho]$ in λ, it follows that its Coulomb, exchange, and correlation contributions can be written as coupling-constant

a)Electronic mail: a.m.teale@kjemi.uio.no. FAX: +47-228-55441.

integrals of the form

$$E_{\mathrm{typ}}[\rho] = \int_0^1 \mathcal{W}_{\mathrm{typ},\lambda}[\rho]\mathrm{d}\lambda, \tag{1}$$

where the AC integrand $\mathcal{W}_{\mathrm{typ},\lambda}[\rho]$ decreases monotonically in λ and "typ" can be Coulomb-exchange-correlation (Jxc), xc, or correlation only (c). An explicit form of the AC integrand is readily derived using the Hellmann–Feynman theorem—for example, $\mathcal{W}_{\mathrm{Jxc},\lambda}[\rho]=\langle\Psi_\lambda|\hat{W}'_\lambda|\Psi_\lambda\rangle$, where the prime denotes differentiation with respect to λ and Ψ_λ is the wave function that yields ρ while minimizing $\hat{T}+\hat{W}_\lambda$. In general, the two-electron interaction can be modified in any manner that smoothly connects the noninteracting and physical systems;[21] for example, using interactions damped by the error function and Gaussian-attenuated error function, see Ref. 22. The shape of the resulting AC curve is thus determined by the variation principle and the choice of the two-electron operator $\hat{W}_\lambda=\Sigma_{i>j}w(r_{ij},\lambda)$. In the present work, we consider only the simplest and most common choice $w(r_{ij},\lambda)=\lambda/r_{ij}$, in which the two-electron interaction is turned on and off by a simple scaling. The derivatives required to evaluate the AC integrand then require only expectation values of the usual two-electron interaction operator, appropriately generalized for nonvariational wave functions.

While the structure of Eq. (1) appears remarkably simple, the complexity of the problem is hidden in the integrand $\mathcal{W}_{\mathrm{Jxc},\lambda}[\rho]$, whose integral up to a given interaction strength yields all the energetic effects of the electron-electron interaction. In the early 1990s, Becke noted that if we can construct a simple AC model in terms of easily computable quantities for $0\leq\lambda\leq1$, then integration of this model with respect to λ yields an xc functional.[23] In the absence of detailed information about the shape of the AC curve, Becke proposed the simplest possible model for the AC integrand—namely, a linear interpolation between the orbital-dependent exchange expression at $\lambda=0$ (the exact value) and a local-spin-density approximation to the $\lambda=1$ point, resulting in the Becke Half and Half (BH&H) functional, obtained by coupling constant integration, containing 50% orbital-dependent exchange. The accuracy of calculated thermochemical quantities for such a functional over a large set of molecules was subsequently improved by semiempirical reduction of the amount of orbital-dependent exchange in the functional, leading to the construction of a whole class of semiempirical hybrid functionals, the most famous of which is the B3LYP functional.[24–28] Typically, these functionals contain between 20% and 30% of the orbital-dependent exchange contribution and arguments based on the AC have been used to justify this practice.[29]

Following the initial development of hybrid functionals, the direct modeling of the AC as a constructive approach to the development of xc functionals was largely abandoned, owing to a lack of detailed knowledge about the behavior of the AC integrand and also to the success of functionals constructed either by semiempirical parametrization of the xc energy or by satisfying various exact theoretical conditions. However, alongside these developments, a number of authors continued to pursue AC modeling, notable attempts include the [1/1]–Padé-based form of Ernzerhof,[6] the two-legged representation of Burke *et al.*,[11] the interaction-strength-interpolation (ISI) model of Seidl *et al.*,[12,13,30,31] and a range of simple forms considered by Mori-Sánchez, Cohen, and Yang.[10] In these works, a form capable of reproducing known properties of the AC curve is first chosen and then approximate input parameters developed. However, this approach leads to several immediate questions: How should we attempt to devise new forms for approximation of the AC curve? Even with exact input information, how accurate can these forms be? What is the impact of specific choices of approximate input parameters on their accuracy?

In the present work, we address the above questions. Recently, we have implemented a method for the calculation of the AC integrands in Eq. (1) from accurate wave-function models of electronic-structure theory, utilizing the procedure proposed by Wu and Yang for maximizing the Lieb functional at different interaction strengths.[32,33] This recourse to the wave function allows the accurate determination of DFT quantities such as the KS orbitals, potential and energy components, and to study their evolution into their interacting counterparts along the AC path. In this work, we demonstrate how this procedure can provide valuable information, enabling the accurate modeling of AC curves. In previous studies,[19,20,33] we focused directly on the behavior of the AC integrand (as have many other authors[6,10–13]), quantifying the accuracy of a variety of previously studied AC forms when their input parameters are chosen so as to reproduce the AC curve at the noninteracting and fully interacting points and the slope of the AC curve at the noninteracting point. Most recently, we compared these forms with accurate curves for all interaction strengths,[33] highlighting error cancellations and aspects requiring improvement. In the present paper, we continue this work, shifting our attention to the development of new models of the AC integrand. By examining the structure of the energy in various electronic-structure theories, we develop models for the interaction-strength dependence of the xc energy in DFT, whose differentiation provides AC models directly. Integration over the coupling constant from zero to λ then gives expressions for the correlation energy along the AC path. These models are assessed by comparison to accurate AC curves, calculated by the Lieb variation principle.

In Sec. II, we first give an overview of Lieb's formulation of DFT, generalized to arbitrary coupling strengths.[15,32,34] In particular, we focus on the applicability of this approach when approximate theories for the determination of the electronic energy and density are employed. The technique used to perform the Lieb maximization and to determine the AC integrand is then briefly reviewed.[32,33] At the end of Sec. II, we consider the KS decomposition of the universal density functional $F_\lambda[\rho]$ and the corresponding maximizing potential v_λ; here, the relation between the density-fixed AC and Görling–Levy perturbation theory is also discussed.

In Sec. III, we apply this methodology to determine the universal density functional $F_\lambda[\rho]$ and the AC integrand for the helium isoelectronic series, the hydrogen molecule, the beryllium isoelectronic series, the neon atom, and the water

molecule using Hartree–Fock (HF) theory, second-order Møller–Plesset (MP2) theory, coupled-cluster singles-and-doubles (CCSD) theory, and coupled-cluster singles-doubles-perturbative-triples [CCSD(T)] theory. The shapes of the resulting AC curves are first discussed in terms of perturbation theory, leading to the development of simple two-parameter doubles (AC-D) and triples (AC-T) AC models, based on considerations of the contributions of virtual double and triple excitations, respectively, to the dynamical correlation energy. Subsequently, for static correlation, a configuration-interaction (CI) analysis of the electronic structure in H_2 leads to a simple CI-based AC model (AC-CI), which is remarkably accurate with only two parameters. The AC-CI model of the AC integrand is applicable also to systems dominated by dynamical correlation, containing to lowest order the previously developed AC-D model.

In Sec. IV, we illustrate how the methodology used to calculate accurate AC curves enables the assessment of xc functionals such as the BLYP functional and AC curves based on the ISI model. The latter uses a simple functional for the AC integrand at infinite interaction strength ($\lambda=\infty$) and we explore the use of this functional to replace the fully interacting point in the AC models of the present work. In Sec. V, we give some concluding remarks and outline future work toward a practical implementation of the family of DFT xc functionals based on these considerations.

II. THEORETICAL BACKGROUND

A. Lieb's formulation of DFT in exact and approximate theories

We now briefly review Lieb's convex-conjugate density functional,[34] introducing from the outset the coupling-strength parameter λ. Consider an N-electron system described by the Hamiltonian (in atomic units)

$$\hat{H}_\lambda[v] = \hat{T} + \lambda\hat{W} + \sum_i v(\mathbf{r}_i) = -\frac{1}{2}\sum_i \nabla_i^2 + \lambda\sum_{i>j}\frac{1}{r_{ij}} + \sum_i v(\mathbf{r}_i), \tag{2}$$

where v is the external potential and where the two-electron interaction $\lambda\hat{W}$ depends linearly on λ. For a noninteracting system, $\lambda=0$; for a fully interacting system, $\lambda=1$; for a strongly interacting or strictly correlated system, $\lambda=\infty$. From this Hamiltonian, we may calculate the ground-state electronic energy $E_\lambda[v]$ exactly or approximately. In exact theory, the ground-state energy (excluding the nuclear-nuclear repulsion energy) is given by

$$E_\lambda[v] = \inf_{\hat{\gamma}\to N} \mathrm{Tr}\,\hat{H}_\lambda[v]\hat{\gamma}, \tag{3}$$

where the minimization is over all ensemble density matrices $\hat{\gamma}$ containing N electrons. From the variation principle, it follows that $E_\lambda[v]$ is concave in v,

$$\begin{aligned} E_\lambda[cv_1 + (1-c)v_2] &= \inf_{\hat{\gamma}\to N}(c\,\mathrm{Tr}\,\hat{H}_\lambda[v_1]\hat{\gamma} + (1-c)\mathrm{Tr}\,\hat{H}_\lambda[v_2]\hat{\gamma}) \\ &\geq c\inf_{\hat{\gamma}\to N}\mathrm{Tr}\,\hat{H}_\lambda[v_1]\hat{\gamma} + (1-c)\inf_{\hat{\gamma}\to N}\mathrm{Tr}\,\hat{H}_\lambda[v_2]\hat{\gamma} \\ &= cE_\lambda[v_1] + (1-c)E_\lambda[v_2], \end{aligned} \tag{4}$$

where $0\leq c\leq 1$. In approximate theories, the electronic energy may be obtained in different ways based on the variation principle or some other criterion. In approximate theories, therefore, the calculated ground-state energy $E_\lambda[v]$ is not necessarily concave in v. However, concavity holds for all models based on the variation principle provided the variational space is the same for all external potentials v. This condition is satisfied, for example, in HF theory in the limit of a complete one-electron basis. Thus, the conditions for concavity are the same as for the Hellmann–Feynman theorem. In general, however, we cannot assume that an approximately calculated electronic energy is concave. Still, as our description is improved—for example, by increasing the one-electron basis set in HF theory—the calculated energy will approach concavity in the potential v.

To illustrate the consequences of nonconcavity in approximate theories, we consider two helium atoms with external potentials,

$$v_A(\mathbf{r}) = -\frac{2}{r_A}, \quad v_B(\mathbf{r}) = -\frac{2}{r_B}. \tag{5}$$

Taking a convex combination of these potentials, we obtain the potential of a hydrogen molecule

$$v_{H_2}(\mathbf{r}) = \frac{1}{2}v_A(\mathbf{r}) + \frac{1}{2}v_B(\mathbf{r}) = -\frac{1}{r_A} - \frac{1}{r_B}. \tag{6}$$

The interpolation characterization of concavity of the ground-state energy (without the nuclear-nuclear repulsion included) in Eq. (4) then implies the relations

$$\begin{aligned} E_\lambda[v_{H_2}] &= E_\lambda\left[\tfrac{1}{2}v_A + \tfrac{1}{2}v_B\right] \\ &\geq \tfrac{1}{2}E_\lambda[v_A] + \tfrac{1}{2}E_\lambda[v_B] = E_\lambda[v_{He}]. \end{aligned} \tag{7}$$

Hence, the exact electronic energy of the hydrogen molecule is (at all internuclear separations) greater than or equal to the energy of the helium atom. However, in approximate calculations of the energies of He and H_2, we typically use finite basis sets, which are different for the two systems (and for different internuclear separations of H_2). Consequently, the energy may jump discontinuously from He to H_2 in a manner that does not satisfy the concavity of Eq. (7).

Following Lieb's treatment,[34] we introduce the universal density functional $F_\lambda[\rho]$ as the Legendre–Fenchel transform (convex conjugate) to the ground-state energy $E_\lambda[v]$,

$$F_\lambda[\rho] = \sup_v\left(E_\lambda[v] - \int v(\mathbf{r})\rho(\mathbf{r})d\mathbf{r}\right), \tag{8}$$

where the Lieb maximization is over a complete vector space of potentials. It is important to note that the density functional $F_\lambda[\rho]$ is convex in ρ by construction, independent of

the concavity of $E_\lambda[v]$ in v. A convex density functional $F_\lambda[\rho]$ may thus be set up at any level of theory, independent of the concavity of $E_\lambda[v]$. However, for a nonconcave, approximate ground-state energy $E_\lambda[v]$, only the concave points of $E_\lambda[v]$ contribute to the maximization in Eq. (8). As a result, $F_\lambda[\rho]$ encapsulates information only about the concave envelope (least concave majorant) to $E_\lambda[v]$.

Subjecting our density functional Eq. (8) to a further Legendre–Fenchel transformation, we arrive at the Hohenberg–Kohn variation principle at the chosen level of theory,

$$\bar{E}_\lambda[v] = \inf_\rho \left(F_\lambda[\rho] + \int v(\mathbf{r})\rho(\mathbf{r})\mathrm{d}\mathbf{r} \right), \tag{9}$$

where the biconjugate $\bar{E}_\lambda[v]$ is the concave envelope to $E_\lambda[v]$,

$$\bar{E}_\lambda[v] \geq E_\lambda[v], \quad (E_\lambda[v] \text{ arbitrary}), \tag{10}$$

$$\bar{E}_\lambda[v] = E_\lambda[v], \quad (E_\lambda[v] \text{ concave}). \tag{11}$$

Consequently, at all levels of theory with a concave energy $E_\lambda[v]$, it is possible to construct a density functional $F_\lambda[\rho]$ by the Lieb variation principle in Eq. (8) that exactly reproduces the ground-state energy $E_\lambda[v]=\bar{E}_\lambda[v]$ in the Hohenberg–Kohn variation principle, Eq. (9), for all v. In theories with a nonconcave energy $E_\lambda[v]$ such as coupled-cluster theory, the density functional in Eq. (8) is still well defined but its subsequent use in the Hohenberg–Kohn variation principle is not guaranteed to reproduce $E_\lambda[v]$, yielding instead an upper bound $\bar{E}_\lambda[v] \geq E_\lambda[v]$. The conjugate relationships between the energy and its associated density functional are thus given by

$$E_\lambda[v] \rightarrow F_\lambda[\rho] \leftrightarrow \bar{E}_\lambda[v] \geq E_\lambda[v]. \tag{12}$$

The same relations of Eq. (12) are valid for excited states but are less useful since such states are in general not concave in the external potential, the requirement of orthogonality to lower-energy states being v-dependent.

In the present paper, we construct the density functional $F_\lambda[\rho]$ by Lieb maximization using the HF, MP2, CCSD, and CCSD(T) wave-function models in large one-electron basis sets with all electrons correlated. We emphasize that each chosen model and basis set, such as the all-electron CCSD/cc-pVQZ model, by Eq. (12) sets up its own universal density functional $F_\lambda[\rho]$, which yields exactly the concave envelope $\bar{E}_\lambda[v]$ of $E_\lambda[v]$ when used in the Hohenberg–Kohn variation principle. In the limit of full configuration-interaction (FCI) in a complete one-electron basis, we recover the exact universal-density functional as normally defined.

B. Lieb maximization

We now discuss how the Lieb maximization in Eq. (8) can be performed practically. This maximization has been studied before. First, in the pioneering work of Colonna and Savin,[15] the Lieb maximization was performed using the (Nelder–Mead) downhill simplex method for a number of two- and four-electron atoms, treating the potential by a form commonly used for pseudopotentials generated to replace atomic cores. Later, introducing a representation for the potential first used in the context of the optimized effective potential method,[35] Wu and Yang[32] proposed to perform the Lieb maximization using the quasi-Newton and Newton procedures and applied this scheme at $\lambda=0$. Following their approach, the potential is parametrized in the following manner:

$$v_\mathbf{c}(\mathbf{r}) = v_{\mathrm{ext}}(\mathbf{r}) + (1-\lambda)v_{\mathrm{ref}}(\mathbf{r}) + \sum_t c_t g_t(\mathbf{r}), \tag{13}$$

where the first term $v_{\mathrm{ext}}(\mathbf{r})$ is the external potential due to the nuclei, the second term $(1-\lambda)v_{\mathrm{ref}}(\mathbf{r})$ contains the Fermi–Amaldi reference potential[36] to ensure a correct asymptotic behavior

$$v_{\mathrm{ref}}(\mathbf{r}) = \left(1 - \frac{1}{N}\right) \int \frac{\rho(\mathbf{r}')}{|\mathbf{r}-\mathbf{r}'|}\mathrm{d}\mathbf{r}', \tag{14}$$

and the final term is a linear expansion in Gaussians $g_t(\mathbf{r})$ with expansion coefficients c_t. For the expansion of the potential in the present work, the same Gaussian basis as for the orbitals is used—namely, the aug-cc-pCVTZ and aug-cc-pCVQZ basis sets[37–40] in uncontracted form (denoted from here on by a prefix u-). Thus, $v_\mathbf{c}(\mathbf{r})$ and hence $F_\lambda[\rho]$ are determined in Eq. (8) by maximizing the quantity

$$G_{\lambda,\rho}(\mathbf{c}) = E_\lambda[v_\mathbf{c}] - \int v_\mathbf{c}(\mathbf{r})\rho(\mathbf{r})\mathrm{d}\mathbf{r} \tag{15}$$

with respect to c_t for a given electronic-structure model $E_\lambda[v_\mathbf{c}]$. Our convergence target is a gradient norm smaller than 10^{-6}. The quasi-Newton method requires only evaluation of the gradient

$$\frac{\partial G_{\lambda,\rho}(\mathbf{c})}{\partial c_t} = \int [\rho_{\lambda,\mathbf{c}}(\mathbf{r}) - \rho(\mathbf{r})] g_t(\mathbf{r})\mathrm{d}\mathbf{r} \tag{16}$$

and converges in 100–200 iterations with the Broyden–Fletcher–Goldfarb–Shanno (BFGS) update. The full Newton method requires also the Hessian with respect to the expansion coefficients

$$\frac{\partial^2 G_{\lambda,\rho}(\mathbf{c})}{\partial c_t \partial c_u} = \int\int g_t(\mathbf{r}) g_u(\mathbf{r}') \frac{\delta\rho(\mathbf{r})}{\delta v(\mathbf{r}')}\mathrm{d}\mathbf{r}\mathrm{d}\mathbf{r}', \tag{17}$$

which is here calculated from CCSD linear response theory,[33] providing expensive but robust convergence in 10–20 iterations at the CCSD and CCSD(T) levels of theory. When using the second-order scheme, we employ a truncated singular-value decomposition with a cutoff of 10^{-6}. For further details of the implementation, see Refs. 32 and 33. All code is implemented in a development version of DALTON.[41]

We note that the Lieb maximization is simple in the sense that few if any global convergence problems are encountered. Indeed, using a simple backtracking mechanism, our implementation of Newton's method converges reliably even with approximate Hessians. The absence of global-convergence problems may be understood from the observation that the exact energy $E_\lambda[v]$ and therefore $E_\lambda[v]-\int v(\mathbf{r})\rho(\mathbf{r})\mathrm{d}\mathbf{r}$ are concave in v, meaning that they con-

tain at most one global (possibly degenerate) maximum. For approximate $E_\lambda[v]$, the situation may be more complicated but we have in no cases observed problems associated with global convergence of the Lieb maximization.

As pointed out in Ref. 32, care must be taken in determining the density $\rho_{\lambda,\mathbf{c}}(\mathbf{r})$ for nonvariational methods. In Lieb's theory, the density is naturally defined as the functional derivative of the energy with respect to the external potential. In the present work, this contribution to Eq. (16) is calculated using the Lagrangian method of Helgaker and Jørgensen,[42–44] yielding the "relaxed" density matrices of MP2, CCSD, and CCSD(T) theories. These relaxed densities are also used for the input physical ($\lambda=1$) densities for these methods.

C. The adiabatic connection

The convex density functional of Lieb[34] in Eq. (8) is equivalent to the Levy–Lieb[34] constrained-search functional for canonical ensembles,

$$F_\lambda[\rho] = \min_{\hat{\gamma}\to\rho} \mathrm{Tr}\, \hat{H}_\lambda[0]\hat{\gamma} = \mathrm{Tr}\, \hat{H}_\lambda[0]\hat{\gamma}^\rho_\lambda, \tag{18}$$

where the minimization is over all density matrices of density ρ ($\hat{\gamma}\to\rho$) and where we have introduced the notation $\hat{\gamma}^\rho_\lambda$ for the minimizing density matrix (which always exists). The functional $F_\lambda[\rho]$ is convex in ρ, concave in λ, and nonnegative for $\lambda\geq 0$. We now relate the interacting functional $F_\lambda[\rho]$ to the corresponding noninteracting quantity $F_0[\rho]$,

$$F_\lambda[\rho] = F_0[\rho] + \int_0^\lambda F'_\lambda[\rho]\mathrm{d}\lambda, \tag{19}$$

where the prime denotes differentiation with respect to the coupling-strength parameter λ. From the concavity of $F_\lambda[\rho]$ in λ, it follows that the integrand $F'_\lambda[\rho]$ is monotonically decreasing in λ. On the right-hand side of Eq. (19), we now insert the expression for the noninteracting energy $F_0[\rho]$ obtained by setting $\lambda=0$ in Eq. (18). Next, we determine $F'_\lambda[\rho]$ by differentiation of Eq. (18) followed by application of the Hellmann–Feynman theorem, leading to the usual AC expression,

$$F_\lambda[\rho] = T_\mathrm{s}[\rho] + \int_0^\lambda \mathcal{W}_{\mathrm{Jxc},\lambda}[\rho]\mathrm{d}\lambda, \tag{20}$$

where the noninteracting kinetic-energy functional and the AC integrand are given by

$$T_\mathrm{s}[\rho] = \mathrm{Tr}\, \hat{H}_0[0]\hat{\gamma}^\rho_0, \tag{21}$$

$$\mathcal{W}_{\mathrm{Jxc},\lambda}[\rho] = \mathrm{Tr}\, \hat{W}\hat{\gamma}^\rho_\lambda, \tag{22}$$

with the density matrix $\hat{\gamma}^\rho_\lambda$ optimized at interaction strength λ from Eq. (18). The expansion of density functional Eq. (20) in λ leads to Görling–Levy perturbation theory.[45,46]

It is customary to decompose the total interaction energy in Eq. (20) in the manner

$$\int_0^\lambda \mathcal{W}_{\mathrm{Jxc},\lambda}[\rho]\mathrm{d}\lambda = \lambda J[\rho] + \lambda E_\mathrm{x}[\rho] + E_{\mathrm{c},\lambda}[\rho], \tag{23}$$

where we have introduced the classical Coulomb functional

$$J[\rho] = \frac{1}{2}\int\int \frac{\rho(\mathbf{r}_1)\rho(\mathbf{r}_2)}{r_{12}}\mathrm{d}\mathbf{r}_1\mathrm{d}\mathbf{r}_2, \tag{24}$$

the exchange functional

$$E_\mathrm{x}[\rho] = \mathrm{Tr}\, \hat{W}\hat{\gamma}^\rho_0 - J[\rho], \tag{25}$$

and the correlation functional

$$E_{\mathrm{c},\lambda}[\rho] = \int_0^\lambda \mathcal{W}_{\mathrm{c},\lambda}[\rho]\mathrm{d}\lambda, \quad \mathcal{W}_{\mathrm{c},\lambda}[\rho] = \mathrm{Tr}\, \hat{W}(\hat{\gamma}^\rho_\lambda - \hat{\gamma}^\rho_0). \tag{26}$$

The total density functional then becomes

$$F_\lambda[\rho] = T_\mathrm{s}[\rho] + \lambda J[\rho] + \lambda E_\mathrm{x}[\rho] + E_{\mathrm{c},\lambda}[\rho]. \tag{27}$$

Since $F_\lambda[\rho]\geq 0$ is concave in λ and since $T_\mathrm{s}[\rho]+\lambda J[\rho]+\lambda E_\mathrm{x}[\rho]\geq 0$ is affine in λ, it follows that $E_{\mathrm{c},\lambda}[\rho]\leq 0$ is concave in λ and that $\mathcal{W}_{\mathrm{Jxc},\lambda}[\rho]$ is monotonically decreasing. Combining the exchange and correlation terms, we obtain the concave xc energy and the monotonically decreasing xc integrand,

$$E_{\mathrm{xc},\lambda}[\rho] = \int_0^\lambda \mathcal{W}_{\mathrm{xc},\lambda}[\rho]\mathrm{d}\lambda, \quad \mathcal{W}_{\mathrm{xc},\lambda}[\rho] = \mathrm{Tr}\, \hat{W}\hat{\gamma}^\rho_\lambda - J[\rho]. \tag{28}$$

The above considerations concerning the behavior of $F_\lambda[\rho]$ and its components hold also for approximate theories when the same ansatz $E_\lambda[v]$ is used for all values of λ, as is trivially satisfied.

D. The effective potential

To understand the AC better, we rewrite the Lieb variation principle, Eq. (8), in the form

$$F_\lambda[\rho] = E_\lambda[v_\lambda] - \int v_\lambda(\mathbf{r})\rho(\mathbf{r})\mathrm{d}\mathbf{r} \Leftrightarrow \frac{\delta F_\lambda[\rho]}{\delta\rho(\mathbf{r})} = -v_\lambda(\mathbf{r}), \tag{29}$$

where $v_\lambda(\mathbf{r})$ is the maximizing potential at coupling strength λ (here assumed to exist). To express $v_\lambda(\mathbf{r})$ in terms of Coulomb, exchange, and correlation contributions, we differentiate Eq. (27) with respect to the density and obtain

$$\frac{\delta F_\lambda[\rho]}{\delta\rho(\mathbf{r})} = \frac{\delta T_\mathrm{s}[\rho]}{\delta\rho(\mathbf{r})} + \lambda v_\mathrm{J}(\mathbf{r}) + \lambda v_\mathrm{x}(\mathbf{r}) + v_{\mathrm{c},\lambda}(\mathbf{r}), \tag{30}$$

where we have introduced the potentials

$$v_\mathrm{J}(\mathbf{r}) = \frac{\delta J[\rho]}{\delta\rho(\mathbf{r})}, \quad v_\mathrm{x}(\mathbf{r}) = \frac{\delta E_\mathrm{x}[\rho]}{\delta\rho(\mathbf{r})}, \quad v_{\mathrm{c},\lambda}(\mathbf{r}) = \frac{\delta E_{\mathrm{c},\lambda}[\rho]}{\delta\rho(\mathbf{r})}, \tag{31}$$

with the limits $v_{\mathrm{c},1}(\mathbf{r})=v_\mathrm{c}(\mathbf{r})$ and $v_{\mathrm{c},0}(\mathbf{r})=0$ for the correlation potential. Introducing the stationary condition $\delta F_\lambda[\rho]/\delta\rho(\mathbf{r})=-v_\lambda(\mathbf{r})$ from Eq. (29) and the corresponding

noninteracting condition $\delta T_s[\rho]/\delta\rho(\mathbf{r}) = -v_s(\mathbf{r})$, we obtain

$$v_\lambda(\mathbf{r}) = v_s(\mathbf{r}) - \lambda v_J(\mathbf{r}) - \lambda v_x(\mathbf{r}) - v_{c,\lambda}(\mathbf{r}), \tag{32}$$

where we note that $v_s(\mathbf{r}) = v_{ext}(\mathbf{r}) + v_J(\mathbf{r}) + v_x(\mathbf{r}) + v_c(\mathbf{r})$ by setting $\lambda = 1$. Eliminating $v_s(\mathbf{r})$, we obtain the following expression for the effective potential:

$$v_\lambda(\mathbf{r}) = v_{ext}(\mathbf{r}) + (1-\lambda)v_J(\mathbf{r}) + (1-\lambda)v_x(\mathbf{r}) + [v_c(\mathbf{r}) - v_{c,\lambda}(\mathbf{r})]. \tag{33}$$

Finally, inserting this potential into the electronic Hamiltonian of Eq. (2), we obtain

$$\hat{H}_\lambda[v_\lambda] = \hat{T} + \sum_i v_{ext}(\mathbf{r}_i) + \lambda\hat{W} + (1-\lambda)\sum_i (v_J(\mathbf{r}_i) + v_x(\mathbf{r}_i)) + \sum_i (v_c(\mathbf{r}_i) - v_{c,\lambda}(\mathbf{r}_i)), \tag{34}$$

where the potential v_λ depends on λ in such a way that the electron density remains constant.

E. Görling–Levy perturbation theory

In Görling–Levy perturbation theory,[45,46] we expand $F_\lambda[\rho]$ in orders of λ about $\lambda = 0$ and obtain

$$F_\lambda[\rho] = T_s[\rho] + \lambda J[\rho] + \lambda E_x[\rho] + E_{c,\lambda}[\rho], \tag{35}$$

$$E_{c,\lambda}[\rho] = -\lambda^2 \sum_{ai} \frac{|\langle a|v_x - \hat{k}_x|i\rangle|^2}{\varepsilon_a - \varepsilon_i} - \frac{\lambda^2}{4}\sum_{ijab} \frac{|\langle ij||ab\rangle|^2}{\varepsilon_a + \varepsilon_b - \varepsilon_i - \varepsilon_j} + \mathcal{O}(\lambda^3), \tag{36}$$

where i, j and a, b denote occupied and virtual orbitals, respectively. We have furthermore introduced the nonmultiplicative exchange operator

$$\hat{k}_x\varphi_p(\mathbf{r}) = -\sum_{i(\mathrm{occ})} \int \frac{\varphi_i^*(\mathbf{r}')\varphi_p(\mathbf{r}')}{|\mathbf{r}-\mathbf{r}'|}\mathrm{d}\mathbf{r}'\,\varphi_i(\mathbf{r}) \tag{37}$$

and the notation

$$\langle pq|rs\rangle = \int\int \varphi_p^*(\mathbf{r}_1)\varphi_q^*(\mathbf{r}_2) r_{12}^{-1} \varphi_r(\mathbf{r}_1)\varphi_s(\mathbf{r}_2)\mathrm{d}\mathbf{r}_1\mathrm{d}\mathbf{r}_2, \tag{38}$$

$$\langle pq||rs\rangle = \langle pq|rs\rangle - \langle pq|sr\rangle. \tag{39}$$

We note that in Eq. (35), the nonlinear terms in λ contribute to $E_{c,\lambda}[\rho]$. Whereas the main contribution to correlation arises from the last quadratic term, the first quadratic term describes the relaxation of the orbitals due to introduction of correlation and, in particular, the replacement of multiplicative exchange and correlation by nonmultiplicative orbital-dependent exchange. Differentiating the second-order Görling–Levy (GL2) energy in Eq. (36), we obtain the expression for the AC integrand,

$$\mathcal{W}_{c,\lambda}[\rho] = -2\lambda \sum_{ai} \frac{|\langle a|v_x - \hat{k}_x|i\rangle|^2}{\varepsilon_a - \varepsilon_i} - \frac{\lambda}{2}\sum_{ijab} \frac{|\langle ij||ab\rangle|^2}{\varepsilon_a + \varepsilon_b - \varepsilon_i - \varepsilon_j} + \mathcal{O}(\lambda^2), \tag{40}$$

where the lowest-order terms depend linearly on λ.

III. THE CALCULATION AND MODELING OF AC CURVES

In this section, we present accurate calculations of AC curves at different levels of theory and for different electronic systems, approximating the resulting curves by simple two-parameter models. We begin by considering the uncorrelated HF wave-function model; next, we consider dynamical correlation at the MP2, CCSD, and CCSD(T) levels of theory, and finally static correlation using FCI theory. All calculations have been carried out in the uncontracted u-aug-cc-pCVQZ basis (with all electrons correlated) except for water, where the smaller u-aug-cc-pCVTZ basis was used.[37–40]

A. The Hartree–Fock model

At interaction strength λ, the HF density functional may be written as

$$F_\lambda^{HF}[\rho] = E_\lambda^{HF}[v_\lambda] - \int \rho(\mathbf{r})v_\lambda(\mathbf{r})\mathrm{d}\mathbf{r}, \quad \rho = \rho_{\lambda=1}^{HF}, \tag{41}$$

where $v_\lambda(\mathbf{r})$ is the effective potential in Eq. (33) corresponding to the stationary condition in Eq. (29). For each λ value, we determine $v_\lambda(\mathbf{r})$ from the Lieb variation principle by expanding the potential in Gaussians according to Eq. (13), as described in Sec. II B. Carrying out Görling–Levy perturbation theory at $\lambda = 0$ under the constraint that the wave function remains a determinant at all interaction strengths λ, we obtain

$$F_\lambda^{HF}[\rho] = T_s[\rho] + \lambda J[\rho] + \lambda E_x[\rho] + E_{c,\lambda}^{HF}[\rho], \tag{42}$$

$$E_{c,\lambda}^{HF}[\rho] = -\lambda^2 \sum_{ai} \frac{|\langle a|v_x - \hat{k}_x|i\rangle|^2}{\varepsilon_a - \varepsilon_i} + \mathcal{O}(\lambda^3), \tag{43}$$

where the negative HF correlation term $E_{c,\lambda}^{HF}[\rho]$ differs from the standard GL2 expression, Eq. (36), by the absence of the (usually dominant) contribution from virtual double excitations.

Consisting entirely of singles contributions, $E_c^{HF}[\rho] = E_{c,1}^{HF}[\rho]$ represents the effect of orbital relaxation upon the introduction of nonmultiplicative exchange in place of multiplicative exchange and correlation. This orbital adjustment is small, as confirmed by the $E_c^{HF}[\rho]$ values listed for the helium isoelectronic series ($1 \le Z \le 10$) in Table I, for the beryllium isoelectronic series ($4 \le Z \le 10$) in Table II, for hydrogen in Table III, for neon in Table IV, and for water in Table V. In fact, for the closed-shell two-electron systems in Tables I and III, $E_c^{HF}[\rho] = 0$, following the observation that the only role of exchange in these systems is to cancel self-interaction. Consequently, the multiplicative exchange potential is equal to $-1/2 v_J(\mathbf{r})$ for such systems for all λ. More generally, for closed-shell two-electron systems, the noninteracting reference system with the HF density is identical to the fully interacting HF system. By contrast, for the four-electron systems in Table II and for the ten-electron systems in Tables IV and V, the HF "correlation energy" $E_c^{HF}[\rho]$ is nonzero but small (of the order of 1 mH) compared with the DFT correlation energies reported in the remaining tables.

TABLE I. KS and wave-function theory energy components for the He isoelectronic series ($Z=1-10$) calculated in the u-aug-cc-pCVQZ basis set. All quantities are in hartree.

Method	Z	$E_{\mathrm{tot}}[v]$	$T[\rho]$	$T_{\mathrm{s}}[\rho]$	$(v\|\rho)$	$\mathcal{W}_1[\rho]$	$J[\rho]$	$E_{\mathrm{x}}[\rho]$	$E_{\mathrm{c}}[\rho]$	$\int_0^1 \mathcal{W}_{\mathrm{xc}} d\lambda$
HF	1	−0.4878	0.4883	0.4883	−1.3722	0.3961	0.7922	−0.3961	0.0000	−0.3961
	2	−2.8615	2.8611	2.8611	−6.7483	1.0257	2.0513	−1.0257	0.0000	−1.0257
	3	−7.2364	7.2364	7.2364	−16.1244	1.6517	3.3034	−1.6517	0.0000	−1.6517
	4	−13.6113	13.6112	13.6112	−29.4995	2.2771	4.5541	−2.2771	0.0000	−2.2771
	5	−21.9862	21.9860	21.9860	−46.8745	2.9023	5.8045	−2.9023	0.0000	−2.9023
	6	−32.3611	32.3609	32.3609	−68.2493	3.5274	7.0548	−3.5274	0.0000	−3.5274
	7	−44.7360	44.7357	44.7357	−93.6242	4.1525	8.3050	−4.1525	0.0000	−4.1525
	8	−59.1110	59.1105	59.1105	−122.9990	4.7775	9.5551	−4.7775	0.0000	−4.7775
	9	−75.4859	75.4853	75.4853	−156.3738	5.4026	10.8052	−5.4026	0.0000	−5.4026
	10	−93.8608	93.8601	93.8601	−193.7486	6.0276	12.0553	−6.0276	0.0000	−6.0276
MP2	1	−0.5171	0.5195	0.5026	−1.3862	0.3495	0.7923	−0.3961	−0.0296	−0.4258
	2	−2.8974	2.8955	2.8677	−6.7545	0.9615	2.0506	−1.0253	−0.0359	−1.0613
	3	−7.2749	7.2737	7.2412	−16.1290	1.5804	3.3029	−1.6515	−0.0385	−1.6900
	4	−13.6513	13.6508	13.6155	−29.5035	2.2014	4.5537	−2.2768	−0.0401	−2.3169
	5	−22.0272	22.0258	21.9887	−46.8769	2.8239	5.8040	−2.9020	−0.0410	−2.9430
	6	−32.4027	32.4009	32.3626	−68.2508	3.4473	7.0543	−3.5271	−0.0416	−3.5687
	7	−44.7780	44.7758	44.7367	−93.6249	4.0711	8.3045	−4.1522	−0.0420	−4.1942
	8	−59.1532	59.1503	59.1107	−122.9989	4.6955	9.5546	−4.7773	−0.0422	−4.8195
	9	−75.5282	75.5251	75.4851	−156.3733	5.3201	10.8047	−5.4023	−0.0423	−5.4446
	10	−93.9033	93.9001	93.8597	−193.7479	5.9445	12.0548	−6.0274	−0.0425	−6.0699
CCSD	1	−0.5271	0.5300	0.5020	−1.3744	0.3173	0.7726	−0.3863	−0.0410	−0.4273
	2	−2.9027	2.9012	2.8650	−6.7505	0.9466	2.0482	−1.0241	−0.0412	−1.0653
	3	−7.2787	7.2775	7.2384	−16.1257	1.5695	3.3018	−1.6509	−0.0423	−1.6932
	4	−13.6543	13.6537	13.6131	−29.5009	2.1929	4.5530	−2.2765	−0.0430	−2.3195
	5	−22.0296	22.0283	21.9868	−46.8748	2.8170	5.8036	−2.9018	−0.0434	−2.9452
	6	−32.4047	32.4030	32.3610	−68.2491	3.4414	7.0540	−3.5270	−0.0436	−3.5706
	7	−44.7798	44.7776	44.7353	−93.6234	4.0660	8.3042	−4.1521	−0.0437	−4.1959
	8	−59.1547	59.1520	59.1095	−122.9976	4.6910	9.5544	−4.7772	−0.0437	−4.8209
	9	−75.5296	75.5266	75.4840	−156.3722	5.3160	10.8046	−5.4023	−0.0437	−5.4460
	10	−93.9046	93.9015	93.8587	−193.7469	5.9408	12.0547	−6.0274	−0.0437	−6.0711

Being small, the HF correlation energy $E_{\mathrm{c}}^{\mathrm{HF}}[\rho]$ should be accurately represented by the lowest-order term in Eq. (43). This expectation is confirmed in Fig. 1, where we have plotted the HF correlation integrand

$$\mathcal{W}_{\mathrm{c},\lambda}^{\mathrm{HF}}[\rho] = \mathrm{Tr}\ \hat{W}(\hat{\gamma}_{\mathrm{s},\lambda}^{\rho} - \hat{\gamma}_{\mathrm{s},0}^{\rho})$$

$$= -2\lambda \sum_{ai} \frac{|\langle a|v_{\mathrm{x}} - \hat{k}_{\mathrm{x}}|i\rangle|^2}{\varepsilon_a - \varepsilon_i} + \mathcal{O}(\lambda^2) \qquad (44)$$

for neon and water. The plotted curves are very nearly linear, indicating that second- and higher-order terms are negligible. In particular, the calculated $E_{\mathrm{c},\lambda}[\rho]$ values (the integrated areas) are −1.7 mH for neon (in the u-aug-cc-pCVQZ basis) and −2.4 mH for water (in the u-aug-cc-pCVTZ basis). For a related analysis of the energy differences between HF calculations and approximate KS calculations yielding the HF density, see the work of Görling and Ernzerhof.[47]

We emphasize that although the HF density functional $F_{\lambda}^{\mathrm{HF}}[\rho]$ in Eq. (41) is defined for all N-representable densities, we have here applied it only to the HF density of the fully interacting system $\rho_{\lambda=1}^{\mathrm{HF}}$. In the following, we shall proceed in the same manner at other levels of theory, working only with densities obtained using the same electronic-structure model as is used for $E_{\lambda}[v]$ in the Lieb functional of Eq. (8). Thus, the noninteracting system at $\lambda=0$ is always represented by a single Slater determinant with the same density as obtained by a standard HF/MP2/CCSD/CCSD(T) calculation at $\lambda=1$. The resulting noninteracting system is therefore different from the usual KS system, designed to give the exact electronic density. However, this approach is consistent with the situation for commonly performed calculations using density-functional approximations (DFAs), where the noninteracting system corresponds to a single Slater determinant constructed from orbitals obtained by minimization of an approximate density functional. The ACs calculated in this work may thus be interpreted as those consistent with DFAs yielding the HF/MP2/CCSD/CCSD(T) electronic densities and energies.

B. The interaction-strength dependence of orbitals and their energies

To prepare for our discussion of MP2 and CCSD theories in Sec. III C, we now consider the variation in orbitals and orbital energies along the HF AC path. For this purpose, we write the density functional in the form

$$F_{\lambda}^{\mathrm{HF}}[\rho] = \min_{\hat{\gamma}_{\mathrm{s}}} \hat{H}_{\lambda}[v_{\lambda}]\hat{\gamma}_{\mathrm{s}} - (v_{\lambda}|\rho) = \min_{\hat{\gamma}_{\mathrm{s}}\to\rho} \hat{H}_{\lambda}[0]\hat{\gamma}_{\mathrm{s}}, \qquad (45)$$

where the constrained minimization over determinantal density matrices $\hat{\gamma}_{\mathrm{s}}\to\rho$ with $\hat{H}[0]$ is equivalent to the uncon

TABLE II. KS and wave-function theory energy components for the Be isoelectronic series (Z=4–10) calculated in the u-aug-cc-pCVQZ basis set. All quantities are in hartree.

Method	Z	$E_{\mathrm{tot}}[v]$	$T[\rho]$	$T_{\mathrm{s}}[\rho]$	$(v\|\rho)$	$\mathcal{W}_1[\rho]$	$J[\rho]$	$E_{\mathrm{x}}[\rho]$	$E_{\mathrm{c}}[\rho]$	$\int_0^1 \mathcal{W}_{\mathrm{xc}} d\lambda$
HF	4	−14.5730	14.5730	14.5724	−33.6350	4.4891	7.1560	−2.6658	−0.0006	−2.6663
	5	−24.2375	24.2376	24.2369	−54.5931	6.1180	9.6102	−3.4909	−0.0007	−3.4916
	6	−36.4083	36.4084	36.4076	−80.5355	7.7188	12.0331	−4.3128	−0.0007	−4.3136
	7	−51.0819	51.0823	51.0816	−111.4723	9.3081	14.4432	−5.1336	−0.0008	−5.1344
	8	−68.2571	68.2582	68.2574	−147.4068	10.8915	16.8470	−5.9539	−0.0008	−5.9547
	9	−87.9331	87.9355	87.9347	−188.3402	12.4716	19.2471	−6.7739	−0.0008	−6.7747
	10	−110.1097	110.1141	110.1133	−234.2733	14.0495	21.6449	−7.5937	−0.0008	−7.5945
MP2	4	−14.6467	14.6454	14.5926	−33.6845	4.3924	7.1907	−2.6709	−0.0746	−2.7455
	5	−24.3223	24.3201	24.2592	−54.6411	5.9988	9.6404	−3.4949	−0.0858	−3.5807
	6	−36.5025	36.4998	36.4325	−80.5855	7.5832	12.0622	−4.3164	−0.0953	−4.4117
	7	−51.1845	51.1818	51.1091	−111.5255	9.1592	14.4726	−5.1369	−0.1038	−5.2407
	8	−68.3673	68.3649	68.2877	−147.4637	10.7316	16.8773	−5.9570	−0.1116	−6.0686
	9	−88.0506	88.0494	87.9683	−188.4018	12.3017	19.2789	−6.7770	−0.1190	−6.8960
	10	−110.2343	110.2351	110.1502	−234.3397	13.8703	21.6783	−7.5967	−0.1264	−7.7231
CCSD	4	−14.6650	14.6643	14.5930	−33.7065	4.3771	7.2157	−2.6735	−0.0938	−2.7674
	5	−24.3461	24.3449	24.2608	−54.6689	5.9779	9.6705	−3.4975	−0.1111	−3.6086
	6	−36.5317	36.5302	36.4352	−80.6192	7.5573	12.0982	−4.3190	−0.1269	−4.4459
	7	−51.2191	51.2179	51.1131	−111.5653	9.1283	14.5148	−5.1396	−0.1422	−5.2818
	8	−68.4074	68.4068	68.2934	−147.5097	10.6955	16.9259	−5.9598	−0.1572	−6.1170
	9	−88.0962	88.0970	87.9756	−188.4536	12.2604	19.3338	−6.7798	−0.1723	−6.9521
	10	−110.2855	110.2882	110.1595	−234.3974	13.8237	21.7396	−7.5996	−0.1876	−7.7872
CCSD(T)	4	−14.6656	14.6649	14.5924	−33.7071	4.3766	7.2171	−2.6735	−0.0945	−2.7681
	5	−24.3468	24.3456	24.2600	−54.6692	5.9769	9.6718	−3.4975	−0.1119	−3.6094
	6	−36.5324	36.5310	36.4343	−80.6194	7.5560	12.0995	−4.3190	−0.1278	−4.4468
	7	−51.2199	51.2187	51.1122	−111.5655	9.1269	14.5161	−5.1396	−0.1432	−5.2828
	8	−68.4083	68.4077	68.2925	−147.5099	10.6940	16.9273	−5.9598	−0.1583	−6.1181
	9	−88.0971	88.0979	87.9748	−188.4538	12.2588	19.3352	−6.7798	−0.1735	−6.9533
	10	−110.2814	110.2891	110.1587	−234.3975	13.8270	21.7411	−7.5996	−0.1840	−7.7886

strained minimization over $\hat{\gamma}_{\mathrm{s}}$ with $\hat{H}_\lambda[v_\lambda]$ in Eq. (34). The latter minimization is carried out in the usual manner by an iterative diagonalization of an effective λ-dependent one-electron operator

$$\hat{f}_\lambda = -\tfrac{1}{2}\nabla^2 + v_{\mathrm{ext}}(\mathbf{r}) + v_{\mathrm{J}}(\mathbf{r}) + (1-\lambda)v_{\mathrm{x}}(\mathbf{r}) + \lambda\hat{k}_{\mathrm{x}} + v_{\mathrm{c}}(\mathbf{r}) - v_{\mathrm{c},\lambda}(\mathbf{r}), \tag{46}$$

with eigenvectors (orbitals) and eigenvalues (orbital energies) that depend on λ,

$$\hat{f}_\lambda \varphi_{p,\lambda}(\mathbf{r}) = \varepsilon_{p,\lambda}\varphi_{p,\lambda}(\mathbf{r}). \tag{47}$$

The effective potential of $\hat{f}_\lambda$ in Eq. (46) follows by application of HF theory to the Hamiltonian $\hat{H}_\lambda[v_\lambda]$ in Eq. (34). In the noninteracting and fully interacting limits, respectively, $\hat{f}_\lambda$ reduces to the KS and Fock operators,

$$\hat{f}_0 = \hat{f}_{\mathrm{KS}} = -\tfrac{1}{2}\nabla^2 + v_{\mathrm{ext}}(\mathbf{r}) + v_{\mathrm{J}}(\mathbf{r}) + v_{\mathrm{x}}(\mathbf{r}) + v_{\mathrm{c}}(\mathbf{r}), \tag{48}$$

TABLE III. KS and wave-function theory energy components for the H_2 molecule calculated in the u-aug-cc-pVQZ basis set. All quantities are in hartree.

Method	R	$E_{\mathrm{tot}}[v]$	E_{nn}	$T[\rho]$	$T_{\mathrm{s}}[\rho]$	$(v\|\rho)$	$\mathcal{W}_1[\rho]$	$J[\rho]$	$E_{\mathrm{x}}[\rho]$	$E_{\mathrm{c}}[\rho]$	$\int_0^1 \mathcal{W}_{\mathrm{xc}} d\lambda$
HF	0.7	−0.8822	1.4286	1.7288	1.7288	−4.8662	0.8267	1.6534	−0.8267	0.0000	−0.8267
	1.4	−1.1335	0.7143	1.1257	1.1257	−3.6320	0.6585	1.3170	−0.6585	0.0000	−0.6585
	3.0	−0.9893	0.3333	0.7125	0.7125	−2.4980	0.4628	0.9257	−0.4628	0.0000	−0.4628
	5.0	−0.8593	0.2000	0.6484	0.6484	−2.0717	0.3640	0.7280	−0.3640	0.0000	−0.3640
	7.0	−0.8018	0.1429	0.6722	0.6722	−1.9424	0.3256	0.6512	−0.3256	0.0000	−0.3256
	10.0	−0.7679	0.1000	0.7032	0.7032	−1.8756	0.3045	0.6090	−0.3045	0.0000	−0.3045
MP2	0.7	−0.9154	1.4286	1.7581	1.7334	−4.8715	0.7694	1.6547	−0.8274	−0.0332	−0.8606
	1.4	−1.1668	0.7143	1.1607	1.1377	−3.6463	0.6046	1.3220	−0.6610	−0.0334	−0.6944
	3.0	−1.0327	0.3333	0.7885	0.7673	−2.5588	0.4042	0.9414	−0.4707	−0.0452	−0.5159
CCSD	0.7	−0.9209	1.4286	1.7650	1.7320	−4.8694	0.7550	1.6535	−0.8268	−0.0387	−0.8655
	1.4	−1.1739	0.7143	1.1740	1.1409	−3.6497	0.5876	1.3226	−0.6613	−0.0407	−0.7020
	3.0	−1.0570	0.3333	0.8705	0.8285	−2.6193	0.3585	0.9546	−0.4773	−0.0768	−0.5541
	5.0	−1.0036	0.2000	0.9750	0.9527	−2.3819	0.2033	0.8195	−0.4098	−0.1841	−0.5939
	7.0	−1.0000	0.1429	0.9980	0.9930	−2.2838	0.1429	0.7671	−0.3836	−0.2357	−0.6193
	10.0	−0.9999	0.1000	0.9996	0.9991	−2.1994	0.1000	0.7248	−0.3624	−0.2619	−0.6244

TABLE IV. KS and wave-function theory energy components for the Ne atom calculated in the u-aug-cc-pCVQZ basis set. All quantities are in hartree.

Method	$E_{tot}[v]$	$T[\rho]$	$T_s[\rho]$	$(v\|\rho)$	$\mathcal{W}_1[\rho]$	$J[\rho]$	$E_x[\rho]$	$E_c[\rho]$	$\int_0^1 \mathcal{W}_{xc} d\lambda$
HF	−128.5451	128.5443	128.5427	−311.1217	54.0323	66.1396	−12.1040	−0.0017	−12.1057
MP2	−128.9110	128.8948	128.5961	−311.0306	53.2248	65.9650	−12.0708	−0.3707	−12.4415
CCSD	−128.9114	128.8972	128.5952	−311.0765	53.2679	66.0196	−12.0799	−0.3698	−12.4499
CCSD(T)	−128.9178	128.9033	128.5879	−311.0456	53.2245	65.9925	−12.0758	−0.3768	−12.4527

$$\hat{f}_1 = \hat{f}_{HF} = -\tfrac{1}{2}\nabla^2 + v_{ext}(\mathbf{r}) + v_J(\mathbf{r}) + \hat{k}_x. \tag{49}$$

Whereas the external and Coulomb potentials are independent of λ, the exchange operator changes smoothly (as a convex combination) from multiplicative exchange at λ=0 to nonmultiplicative exchange at λ=1. At the same time, the correlation potential changes from $v_c(\mathbf{r})$ for λ=0 to zero for the fully interacting potential.

As a result of the transition from multiplicative to nonmultiplicative exchange with increasing λ, the orbital energies are affected in a characteristic manner, as illustrated in Fig. 2, where we have plotted the orbital energies of the neon atom against λ. In the noninteracting limit, electrons in virtual and occupied orbitals experience the same potential, generated by the remaining $N-1$ electrons in the system. In the interacting limit, an electron in an occupied orbital still experiences an effective potential generated by $N-1$ electrons, but an electron in a virtual orbital now experiences an N-electron interaction, thereby raising the energy of the virtual orbitals relative to those in the occupied orbitals. The resulting opening of the highest occupied molecular orbital-lowest unoccupied molecular orbital (HOMO-LUMO) gap has important consequences for the shape of the AC curve at correlated levels of theory, as discussed in Sec. III C.

C. The MP2 and CCSD AC correlation curves

Having studied the HF model, we turn our attention to the dynamically correlated MP2 and CCSD models, for which we expect much larger correlation contributions than in HF theory. In Fig. 3, we have plotted the MP2 and CCSD AC correlation curves for neon (in the u-aug-cc-pCVQZ basis) and water (in the u-aug-cc-pCVTZ basis) with all electrons correlated,

$$F_\lambda^{MP2}[\rho] = E_\lambda^{MP2}[v_\lambda] - \int \rho(\mathbf{r}) v_\lambda(\mathbf{r}) d\mathbf{r}, \quad \rho = \rho_{\lambda=1}^{MP2}, \tag{50}$$

$$F_\lambda^{CCSD}[\rho] = E_\lambda^{CCSD}[v_\lambda] - \int \rho(\mathbf{r}) v_\lambda(\mathbf{r}) d\mathbf{r}, \quad \rho = \rho_{\lambda=1}^{CCSD}, \tag{51}$$

where we use the MP2 and CCSD densities calculated at λ=1, but note that both functionals are applicable to any N-representable density. The effective potentials $v_\lambda(\mathbf{r})$ used in Eqs. (50) and (51) are the maximizing potentials in the Lieb variation principle at interaction strength λ. Since the nonvariational MP2 and CCSD methods do not provide variationally determined Hermitian one-electron density matrices, we have calculated the densities from the corresponding Lagrangian "relaxed" density matrices.[42,44]

For the neon atom, the MP2/u-aug-cc-pCVQZ correlation energy is −366 mH relative to the HF reference state, 22 mH above the basis-set limit of −388 mH. For water, we use the smaller u-aug-cc-CVTZ basis, which gives an MP2 correlation energy of −328 mH, compared with −361 mH in the basis-set limit. It would be possible to reduce the basis-set error by an order of magnitude by performing basis-set extrapolations,[48,49] as done in Ref. 33. However, we here focus on the shape of the AC curve and behavior of the universal energy functionals rather than the absolute values of the basis-set limit energies. The above basis sets, uncontracted and augmented with diffuse basis functions, are sufficiently flexible to provide an accurate representation of the effective potentials $v_\lambda(\mathbf{r})$ and the range of densities considered in the present work—see later for a more detailed analysis.

In agreement with the discussion of the HF model in Sec. III A, we note that the MP2 and CCSD correlation energies calculated relative to the HF energy differ from those obtained by integration of the AC curve, relative to the noninteracting KS energy. Thus, at the MP2/u-aug-cc-pCVQZ level of theory, the neon correlation energies are −366 and −371 mH, respectively, relative to the HF and KS reference energies. The correlation energy is higher relative to the HF energy since this energy is, by definition, the lowest attainable with a single-determinant reference state. Likewise, for

TABLE V. KS and wave-function theory energy components for the H_2O molecule calculated in the u-aug-cc-pCVTZ basis set. The nuclear-nuclear repulsion energy is $9.1969E_h$. All quantities are in hartree.

Method	$E_{tot}[v]$	$T[\rho]$	$T_s[\rho]$	$(v\|\rho)$	$\mathcal{W}_1[\rho]$	$J[\rho]$	$E_x[\rho]$	$E_c[\rho]$	$\int_0^1 \mathcal{W}_{xc} d\lambda$
HF	−76.0617	75.9866	75.9843	−199.0375	37.7922	46.7374	−8.9404	−0.0024	−8.9429
MP2	−76.3892	76.3544	76.1103	−199.1093	37.1687	46.6633	−8.9161	−0.3343	−9.2505
CCSD	−76.3945	76.3545	76.0991	−199.1261	37.1802	46.6985	−8.9249	−0.3381	−9.2629
CCSD(T)	−76.4033	76.3729	76.0996	−199.1050	37.1318	46.6735	−8.9205	−0.3479	−9.2686

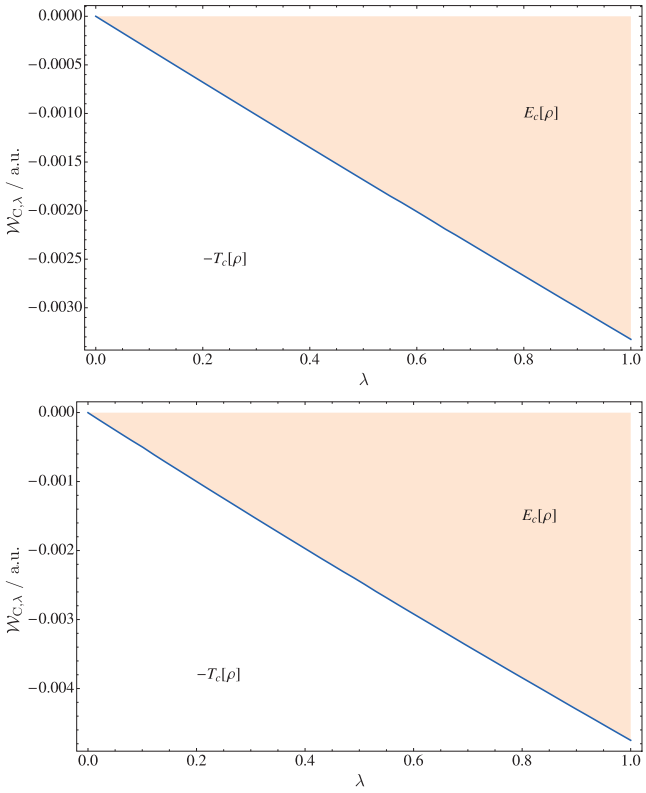

FIG. 1. The AC correlation curve at the HF/u-aug-cc-pCVQZ level of theory for Ne (top) and the HF/u-aug-cc-pCVTZ level of theory for H_2O (bottom).

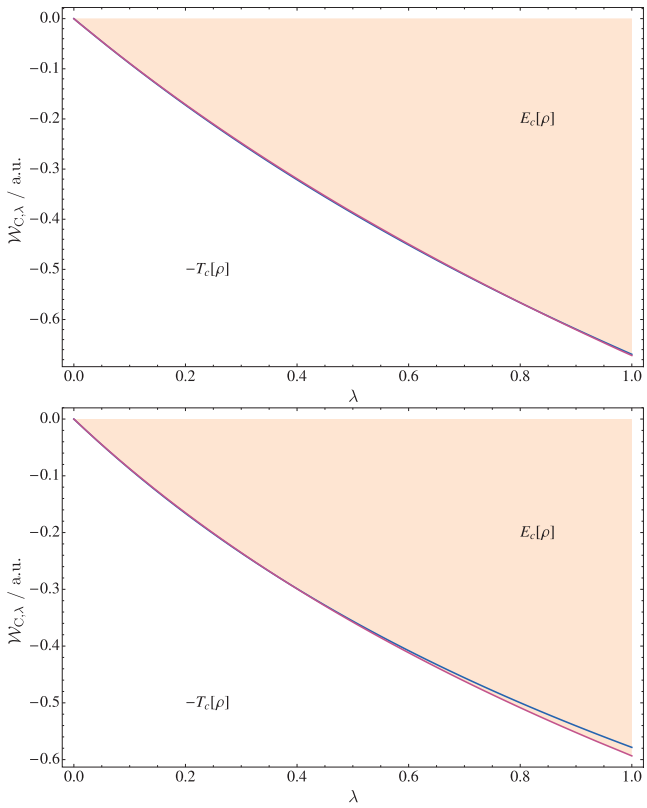

FIG. 3. The AC correlation curve at the all-electron MP2 and CCSD levels of theory for Ne in the u-aug-cc-pCVQZ basis sets (top) and for H_2O in the u-aug-cc-pCVTZ basis (bottom). The MP2 and CCSD curves may be distinguished by noting that the MP2 curve falls below the CCSD curve for all λ values.

water, the correlation energies are −328 and −332 mH, respectively, relative to the HF and KS reference energies.

Apart from their much larger absolute values, the MP2 and CCSD plots in Fig. 3 are significantly more curved than the corresponding HF plots in Fig. 1. Clearly, GL2 theory [see Eq. (40)] strongly overestimates the absolute value of the dynamical correlation energy in neon and water. To describe the curvature of the AC integrand within the framework of Görling–Levy perturbation theory, we must go to third and higher orders in the expansion. Alternatively, we may consider the direct evaluation of $F_\lambda^{\mathrm{MP2}}[\rho]$ from the effective potential $v_\lambda(\mathbf{r})$ in Eq. (50). In MP2 theory, such a calculation is performed by carrying out an initial HF calculation with the Hamiltonian $\hat{H}_\lambda[v_\lambda]$, followed by an MP2 calculation with $\hat{f}_\lambda$ of Eq. (46) as the zero-order Hamiltonian,

$$F_\lambda^{\mathrm{MP2}}[\rho] = \min_{\hat{\gamma}_s} \hat{H}[v_\lambda]\hat{\gamma}_s - (v_\lambda|\rho) - \lambda^2 \sum_{ijab} \frac{|\langle i_\lambda j_\lambda || a_\lambda b_\lambda \rangle|^2}{\varepsilon_{a,\lambda} + \varepsilon_{b,\lambda} - \varepsilon_{i,\lambda} - \varepsilon_{j,\lambda}}, \tag{52}$$

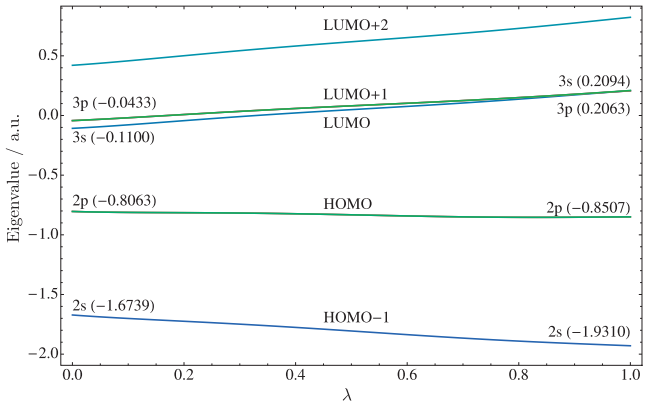

FIG. 2. Orbital energies for neon as a function of interaction strength λ calculated using the u-aug-pCVQZ basis set. The smooth linear variation in the eigenvalues and the opening of the HOMO-LUMO gap reflect the evolution of the multiplicative KS xc operator into the nonmultiplicative HF exchange operator with increasing λ.

where orbitals and orbital energies depend on λ, unlike in the GL2 expansion of Eq. (35), which uses quantities calculated exclusively at λ=0. Assuming that the HOMO-LUMO gap increases linearly with λ (as appears reasonable from the plots in Fig. 2), we arrive at the following simple model that captures the essence of the λ dependence of the MP2 correlation contribution:

$$\mathcal{E}_{\mathrm{D}}(\lambda) = -\frac{w^2\lambda^2}{h + g\lambda}. \tag{53}$$

In the numerator, w represents the interaction of the HF state with excited states present in the numerator of Eq. (52); in the denominator, $h>0$ models the HOMO-LUMO gap in the noninteracting limit in the denominator of Eq. (52), while $g>0$ models the opening of the HOMO-LUMO gap in the presence of electronic interactions. As λ increases, we thus have two competing effects on the correlation energy: a qua-

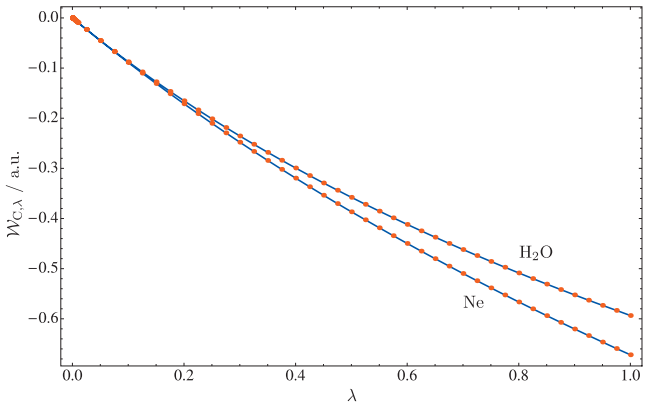

FIG. 4. The AC curves at the all-electron CCSD level of theory in the u-aug-cc-pCVQZ basis sets for neon and water. The calculated curves are represented by dots, whereas curves in Eq. (55) are represented by full lines.

dratic increase in the numerator in Eq. (53) counteracted by a linear increase in the denominator.

To obtain a model for the AC integrand, we differentiate Eq. (53) with respect to λ and obtain

$$\mathcal{E}_{\mathrm{D}}'(\lambda) = -\frac{w^2\lambda(2h+g\lambda)}{(h+g\lambda)^2}. \tag{54}$$

Introducing the parameters $s=-2g^2/h<0$ and $a=-g<0$, we arrive at the following model for the AC integrand:

$$\mathcal{W}_{\text{AC-D}}(\lambda) = \frac{as\lambda(4a+s\lambda)}{(2a+s\lambda)^2} = s\lambda + \mathcal{O}(\lambda^2), \tag{55}$$

where we have also made the assumption $w=g$. The resulting AC integrand $\mathcal{W}_{\text{AC-D}}(\lambda)$ is convex in λ and decreases monotonically from $\lambda=0$ to $\lambda=\infty$ with special values and derivatives,

$$\mathcal{W}_{\text{AC-D}}(0) = 0, \quad \mathcal{W}_{\text{AC-D}}(\infty) = a, \tag{56}$$

$$\mathcal{W}'_{\text{AC-D}}(0) = s, \quad \mathcal{W}'_{\text{AC-D}}(\infty) = 0. \tag{57}$$

Thus, whereas s represents the initial slope of $\mathcal{W}_{\text{AC-D}}(\lambda)$, a represents its asymptotic value in the strongly interacting limit $\lambda=\infty$. By adjusting $a<0$, it is possible to modify $\mathcal{W}_{\text{AC-D}}(\lambda)$ so as to give a selected value $t>s$ for the fully interacting system $\lambda=1$,

$$a = \frac{s^2-4st+s\sqrt{s^2+8st}}{8(t-s)} \Rightarrow \mathcal{W}_{\text{AC-D}}(1) = t > s. \tag{58}$$

An expression in agreement with GL2 theory ($t=s$) is obtained by setting $a=-\infty$. Finally, expressing the correlation energy of Eq. (53) in terms of s and a, we obtain

$$\mathcal{E}_{\text{AC-D}}(\lambda) = \frac{as\lambda^2}{2a+s\lambda}, \tag{59}$$

which for small s is quadratic in λ with curvature $s/2$ and for large s linear in λ with slope a.

In Fig. 4, we compare the calculated CCSD AC curves of neon and water (represented by dots) with the fitted curves, Eq. (55), obtained by adjusting s to the calculated slope at $\lambda=0$ and a to fit the calculated value at $\lambda=1$ using Eq. (58). All fitting and integration of the calculated AC curves in the present work has been carried out using the MATHEMATICA program.[50] The agreement is nearly perfect, confirming that the AC form in Eq. (55) based on the energy model in Eq. (53) captures the physics of dynamical correlation. (Here we have used the CCSD slope and end point, but an equally good fit can be obtained to the MP2 curves using the MP2 data.) Thus, the curvature of the AC integrand in dynamically correlated systems such as neon and water arises from the λ dependence of the HOMO-LUMO gap in the denominator of Eq. (53).

The MP2 and CCSD energy components for the helium isoelectronic series, the beryllium isoelectronic series, hydrogen, neon, and water are presented in Tables I–V, respectively. The MP2 and CCSD correlation energies are similar, the MP2 values being generally slightly smaller in magnitude than those calculated at the CCSD level of theory, although this ordering is sometimes reversed in the basis-set limit.[42]

For the helium isoelectronic series, the CCSD model is equivalent to the FCI model, and the well-known saturation of the correlation energy toward a constant value[51] is evident in Table I. In contrast, for the beryllium isoelectronic series, the correlation energy is known to decrease linearly[51] with increasing Z, as is evident in Table II. The CCSD results for H_2 in Table III also correspond to FCI values and differ by less than 0.1 mH from the aug-cc-pVQZ results in Ref. 33, indicating that uncontraction is unimportant for this molecule. However, for Ne and H_2O in Tables IV and V, respectively, basis-set uncontraction is essential to obtain agreement between the nuclear-electron and Coulomb energies calculated for the input physical density and the densities calculated at each λ point along the AC path. The effect is particularly pronounced for the nuclear-electron attraction energy. With the basis set employed in the present work, these energies agree to better than 0.2 mH, providing a good test of the accuracy of the procedure at all interaction strengths.

D. The CCSD(T) AC correlation curves

As illustrated in Fig. 4, the two-parameter model $\mathcal{W}_{\text{AC-D}}(\lambda)$ given in Eq. (55) is remarkably successful in describing dynamical correlation arising from virtual double excitations. We now proceed to consider the effects of virtual triple excitations at the CCSD(T) level of theory. In Figs. 5 and 6, we have plotted the CCSD and CCSD(T) AC curves and their differences for neon and water, respectively. As expected, the CCSD(T) curve is slightly lower than the CCSD curve in both cases. Moreover, with increasing λ, the difference between the CCSD(T) and CCSD curves increases, reflecting an increasing significance of triples with increasing coupling strength.

To derive a triples model for the AC integrand, we follow the same approach as for the doubles in Eq. (53). From a consideration of the form of the triples correction in CCSD(T) theory,[42] we obtain the expression

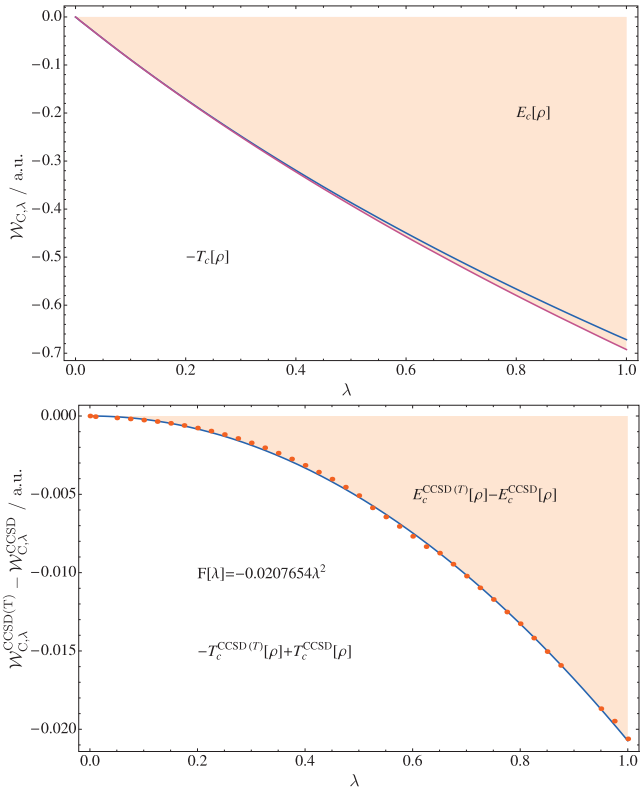

FIG. 5. The AC correlation curve for neon at the all-electron CCSD and CCSD(T) levels of theory in the u-aug-cc-pCVQZ basis sets. In the upper panel, we have plotted the CCSD and CCSD(T) curves separately. In the lower panel, the dots represent the calculated triples corrections, whereas the full line is a quadratic curve of $-0.0208\lambda^2$ fitted to these energy corrections.

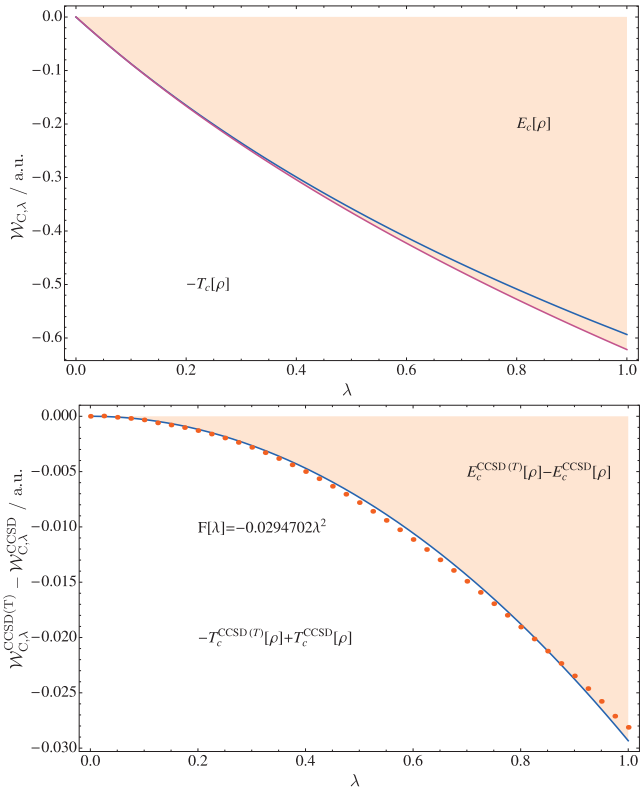

FIG. 6. The AC correlation curve for water at the all-electron CCSD and CCSD(T) levels of theory in the u-aug-cc-pCVTZ basis sets. In the upper panel, we have plotted the CCSD and CCSD(T) curves separately. In the lower panel, the dots represent the calculated triples corrections, whereas the full line is a quadratic curve of $-0.0295\lambda^2$ fitted to these energy corrections.

$$\mathcal{E}_T(\lambda) = -\frac{w^3\lambda^3}{(h+g\lambda)^2}, \tag{60}$$

where w, h, and g have the same significance as for the doubles contribution in Eq. (53). In particular, we note an initial cubic rather than quadratic dependence of the triples correction on λ, explaining the increasing relative importance of the triples correction for large interaction strengths λ. Differentiating Eq. (60) with respect to λ, we obtain

$$\mathcal{E}_T'(\lambda) = -\frac{w^3\lambda^2(3h+g\lambda)}{(h+g\lambda)^3}. \tag{61}$$

Performing the same simplification as for the doubles, we now set $w=g$ and reparametrize Eq. (60) in terms of $c=-6g^3/h^2<0$ and $a=-g<0$, yielding the following triples model AC (AC-T) integrand:

$$\mathcal{W}_{\text{AC-T}}(\lambda) = -\frac{ac\lambda^2(3\sqrt{-6a}+\sqrt{-c}\lambda)}{(\sqrt{-6a}+\sqrt{-c}\lambda)^3}$$

$$= \frac{1}{2}c\lambda^2 + \mathcal{O}(\lambda^3), \quad a<0, \ c<0. \tag{62}$$

Like $\mathcal{W}_{\text{AC-D}}(\lambda)$, the AC integrand $\mathcal{W}_{\text{AC-T}}(\lambda)$ decreases monotonically from $\lambda=0$ to $\lambda=\infty$ with special values,

$$\mathcal{W}_{\text{AC-T}}(0)=0, \quad \mathcal{W}_{\text{AC-T}}(\infty)=a, \tag{63}$$

$$\mathcal{W}'_{\text{AC-T}}(0)=0, \quad \mathcal{W}'_{\text{AC-T}}(\infty)=0, \tag{64}$$

$$\mathcal{W}''_{\text{AC-T}}(0)=c, \quad \mathcal{W}''_{\text{AC-T}}(\infty)=0. \tag{65}$$

Thus, c represents the initial curvature, whereas a represents the asymptotic value. The function is concave for $\lambda<\sqrt{2a/3c}$ and convex for $\lambda>\sqrt{2a/3c}$.

It is possible to adjust a uniquely in Eq. (62) so as to give a selected value t in the range $0>t>c/2$ for the fully interacting system $\lambda=1$. However, for systems dominated by dynamical correlation, the triples correction is small. For example, the triples corrections for neon and water are -6.4 and -8.8 mH, respectively, while the doubles corrections are -372 and -342 mH. The triples correction is therefore accurately described by the lowest-order term $c\lambda^2/2$ in Eq. (62), as demonstrated by the lower plots in Figs. 5 and 6.

E. Static correlation and near degeneracy in the H_2 molecule

To examine the effect of static correlation, we model H_2 in a minimal basis consisting of a bonding $1\sigma_g$ orbital and an antibonding $1\sigma_u$ orbital. In the basis of the doubly occupied $|1\sigma_g^2\rangle$ and $|1\sigma_u^2\rangle$ determinants, the CI Hamiltonian is given by

$$\mathbf{H} = \begin{pmatrix} \langle 1\sigma_g^2|\hat{H}|1\sigma_g^2\rangle & \langle 1\sigma_g^2|\hat{H}|1\sigma_u^2\rangle \\ \langle 1\sigma_u^2|\hat{H}|1\sigma_g^2\rangle & \langle 1\sigma_u^2|\hat{H}|1\sigma_u^2\rangle \end{pmatrix} = \begin{pmatrix} E_g & \lambda w \\ \lambda w & E_u \end{pmatrix}, \tag{66}$$

where w represents the interaction of the HF ground state $|\sigma_g^2\rangle$ and the doubly excited state $|\sigma_u^2\rangle$. Near equilibrium, $E_g<E_u$; at infinite separation, $E_g=E_u$. Taking the lowest eigen-

value of Eq. (66) and subtracting the HF ground-state energy E_g, we obtain the CI correlation energy,

$$\mathcal{E}_{CI} = \tfrac{1}{2}(E_u - E_g) - \tfrac{1}{2}\sqrt{(E_u - E_g)^2 + 4w^2\lambda^2}. \tag{67}$$

Following our approach for MP2, we express the differences between the energies as

$$E_u - E_g = h + g\lambda, \tag{68}$$

where we assume that h and g are both positive. We then obtain the following expression for the correlation energy in terms of the three parameters h, g, and w:

$$\mathcal{E}_{CI}(\lambda) = \tfrac{1}{2}(h + g\lambda) - \tfrac{1}{2}\sqrt{(h + g\lambda)^2 + 4w^2\lambda^2}. \tag{69}$$

Expanding this expression in orders of w, we obtain

$$\mathcal{E}_{CI}(\lambda) = -\frac{w^2\lambda^2}{h + g\lambda} + \mathcal{O}(w^4). \tag{70}$$

As expected, for small w, the CI correlation energy reduces to the perturbative MP2 correlation energy $\mathcal{E}_D(\lambda)$ in Eq. (53).

To determine the corresponding AC integrand, we proceed as for $\mathcal{E}_D(\lambda)$. Differentiation of Eq. (69) with respect to λ yields

$$\mathcal{E}'_{CI}(\lambda) = \frac{1}{2}g - \frac{g(h + g\lambda) + 4w^2\lambda}{2\sqrt{(h + g\lambda)^2 + 4w^2\lambda^2}}. \tag{71}$$

Next, we set $w=g$ and introduce $s=-2g^2/h<0$ and $a=(1-\sqrt{5})g/2<0$, yielding

$$\mathcal{W}_{AC\text{-}CI}(\lambda) = -\frac{1+\sqrt{5}}{4}a - \frac{4(2+\sqrt{5})a^2 + 5(3+\sqrt{5})as\lambda}{2\sqrt{8(7+3\sqrt{5})a^2 + 16(2+\sqrt{5})as\lambda + 10(3+\sqrt{5})s^2\lambda^2}}, \tag{72}$$

where s and a are both negative. The AC integrand $\mathcal{W}_{AC\text{-}CI}(\lambda)$ is convex in λ and decreases monotonically from $\lambda=0$ to $\lambda=\infty$ with special values,

$$\mathcal{W}_{AC\text{-}CI}(0) = 0, \quad \mathcal{W}_{AC\text{-}CI}(\infty) = a, \tag{73}$$

$$\mathcal{W}'_{AC\text{-}CI}(0) = s, \quad \mathcal{W}'_{AC\text{-}CI}(\infty) = 0. \tag{74}$$

It is possible to select $a<0$ uniquely so that $\mathcal{W}_{AC\text{-}CI}(\lambda)$ gives a selected value $t>s$ for the fully interacting system $\lambda=1$, noting that $\mathcal{W}_{AC\text{-}CI}(\lambda)$ increases monotonically with increasing $-\infty<a<0$. However, the explicit formula is rather involved and therefore not given here. Expressing $\mathcal{E}_{CI}(\lambda)$ of Eq. (69) in terms of s and a, we obtain

$$\mathcal{E}_{AC\text{-}CI}(\lambda) = \frac{4a^2 + (\sqrt{5}-1)as\lambda + a\sqrt{16a^2 + 8(\sqrt{5}-1)as\lambda - 10(\sqrt{5}-3)s^2\lambda^2}}{2(\sqrt{5}-3)s}, \tag{75}$$

which may be used to calculate the correlation energy directly from the initial slope s and the strongly interacting limit a of the AC integrand. We note that in the limit of large s (static correlation), $\mathcal{E}_{AC\text{-}CI}(\lambda)$ becomes linear and $\mathcal{W}_{AC\text{-}CI}(\lambda)$ constant in λ. Conversely, in the limit of small s (dynamical correlation), $\mathcal{E}_{AC\text{-}CI}(\lambda)$ becomes quadratic and $\mathcal{W}_{AC\text{-}CI}(\lambda)$ linear λ.

In Fig. 7, we compare $\mathcal{W}_{AC\text{-}D}(\lambda)$, $\mathcal{W}_{AC\text{-}T}(\lambda)$, and $\mathcal{W}_{AC\text{-}CI}(\lambda)$ curves, calculated from Eqs. (55), (62), and (72), respectively, using $s,c=-1$, chosen to give $-1/3$ at $\lambda=\infty$ (top plots) or at $\lambda=1$ (bottom plots). All curves decrease monotonically from zero toward the asymptotic value. Whereas $\mathcal{W}_{AC\text{-}D}(\lambda)$ and $\mathcal{W}_{AC\text{-}CI}(\lambda)$ are everywhere convex, $\mathcal{W}_{AC\text{-}T}(\lambda)$ is first concave then convex.

In Figs. 8 and 9, we compare the $\mathcal{W}_{AC\text{-}CI}(\lambda)$ model and the $\mathcal{W}_{AC\text{-}D}(\lambda)$ model, respectively, with the FCI/u-aug-cc-pCVQZ values of $\mathcal{W}^{CI}_{\lambda,c}[\rho_{FCI}]$ for H_2 at different internuclear separations. For each model, the parameters s and a of Eqs. (55) and (72) were determined in two different ways. The full lines were obtained by a least-squares fit of s and a to all calculated FCI values. For the AC-CI model in Fig. 8, this approach gives an essentially perfect fit to the calculated FCI values at all internuclear separations, confirming that the simple two-parameter model in Eq. (55) captures all the essential physics of dynamical correlation (at short bond distances) and static correlation (at long bond distances). Somewhat surprisingly, the AC-D model in Eq. (55) provides an almost equally good representation of the AC curves in Fig. 9, giving slightly too high AC values in the intermediate λ region. However, since $\mathcal{W}_{AC\text{-}D}(\lambda)$ and $\mathcal{W}_{AC\text{-}CI}(\lambda)$ are both two-parameter models, we advocate the use of the AC-CI model in Eq. (72) for the modeling of AC curves.

The dashed lines in Figs. 8 and 9, respectively, represent the same models $\mathcal{W}_{AC\text{-}CI}(\lambda)$ and $\mathcal{W}_{AC\text{-}D}(\lambda)$ but with the parameters s and a selected in a different manner, setting s equal to the FCI/u-aug-cc-pCVQZ slope at $\lambda=0$ and adjusting a so as to reproduce the FCI/u-aug-cc-pCVQZ value at $\lambda=1$. The curves constructed in this manner necessarily provide poorer global fits to the calculated FCI curves than do the least-squares fits but have the advantage of requiring less data for their construction—namely, only the initial gradient and the end-point value. We note from Fig. 8 that the $\mathcal{W}_{AC\text{-}CI}(\lambda)$ model still provides a very good fit to the calculated AC curves, whereas the $\mathcal{W}_{AC\text{-}D}(\lambda)$ model in Fig. 9 pro-

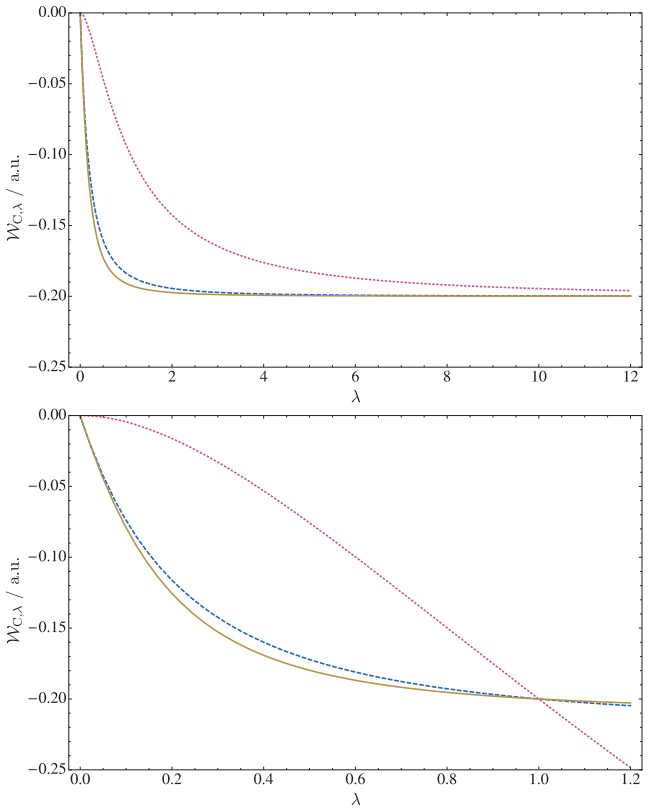

FIG. 7. Comparison of $\mathcal{W}_{\text{AC-D}}(\lambda)$ (dashed line), $\mathcal{W}_{\text{AC-T}}(\lambda)$ (dotted line), and $\mathcal{W}_{\text{AC-CI}}(\lambda)$ (full line) of Eqs. (55), (62), and (72), respectively, with $s=-1$ or $c=-1$. In the top plots, $a=-1/3$; in the bottom plots, a is adjusted to give the same value $(-1/3)$ at $\lambda=1$.

vides a significantly poorer representation of the AC curve than that obtained by least-squares fitting, demonstrating the superiority of the AC-CI model for this system.

IV. USE OF AC CURVES TO ANALYZE EXCHANGE–CORRELATION FUNCTIONALS

In the previous Secs. III C and III D, we have shown how we may derive AC forms with sufficient flexibility to capture a range of correlation effects by considering the structure of the energy expressions arising in wave-function methodologies for varying interaction strength. In particular, we have focused on their accuracy when fitted to high-quality *ab initio* data. Here, we examine two examples of how xc functionals may be usefully analyzed in terms of their AC curves.

A. The BLYP functional

First, we consider the BLYP functional.[24,25] This generalized-gradient-approximation (GGA) functional consists of the Dirac exchange functional, the Becke-88X (B88X) GGA exchange correction,[24] and the Lee–Yang–Parr (LYP) correlation functional.[25] As for orbital-dependent DFT exchange, these exchange terms change linearly with λ and so the corresponding AC curve is horizontal. The LYP functional, in contrast, has a more complicated behavior with respect to variations in λ. However, the corresponding AC curve can be derived from scaling relations using the general formula

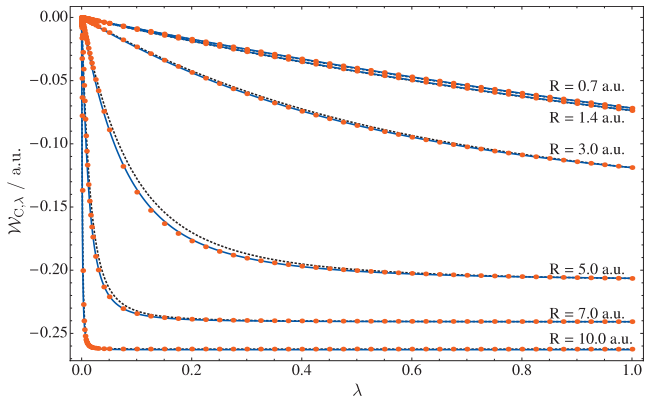

FIG. 8. The AC-CI two-parameter AC model $\mathcal{W}_{\text{AC-CI}}(\lambda)$ of Eq. (72) (full and dashed lines) compared with FCI/u-aug-cc-pCVQZ values of $\mathcal{W}^{\text{CI}}_{\lambda,c}[\rho_{\text{FCI}}]$ (plotted points) for H_2 at different internuclear separations R. The full line was obtained by a least-squares fit of s and a in Eq. (72) to all calculated FCI values; the dashed line was obtained by setting s equal to the FCI gradient at $\lambda=0$ and by adjusting a to reproduce the FCI value at the end point $\lambda=1$.

$$\mathcal{W}_{c,\lambda}[\rho_{1/\lambda}] = 2\lambda E_c[\rho_{1/\lambda}] + \lambda^2 \frac{\partial E_c[\rho_{1/\lambda}]}{\partial \lambda}, \tag{76}$$

where $\rho_{1/\lambda}(\mathbf{r}) = \lambda^{-3}\rho(\mathbf{r}/\lambda)$ is the coordinate-scaled density.[52–54] Derivatives of the AC curves for particular choices of xc functional can be obtained by differentiating this expression with respect to λ. Explicit formulas for the LYP correlation functional are given in the Appendix of Ref. 10.

The BLYP AC curve was implicitly used in the construction of the Mori-Sanchéz–Cohen–Yang (MCY) family of functionals,[9] which are based on model AC curves that intercept the BLYP curve at $\lambda=\lambda_p$ and have an initial slope given by a modified Tao–Perdew–Staroverov–Scuseria functional.[9,55] The functional performance is found to vary significantly with the choice of λ_p, which was chosen to be 0.63. The MCY1 functional, in particular, is based on a [1/1]-Padé form for the integrand with the input parameters as above; the same form with a different parametrization was

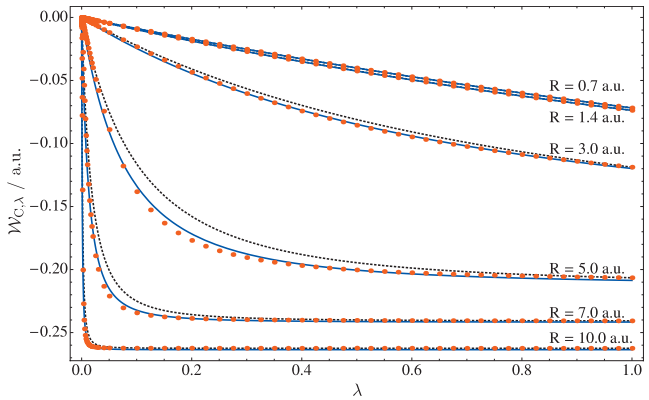

FIG. 9. The AC-D two-parameter AC model $\mathcal{W}_{\text{AC-D}}(\lambda)$ of Eq. (55) (full and dashed lines) compared with FCI/u-aug-cc-pCVQZ values of $\mathcal{W}^{\text{CI}}_{\lambda,c}[\rho_{\text{FCI}}]$ (plotted points) for H_2 at different internuclear separations R. The full line was obtained by a least-squares fit of s and a in Eq. (55) to all calculated FCI values; the dashed line was obtained by setting s equal to the FCI gradient at $\lambda=0$ and by adjusting a to reproduce the FCI value at the end point $\lambda=1$.

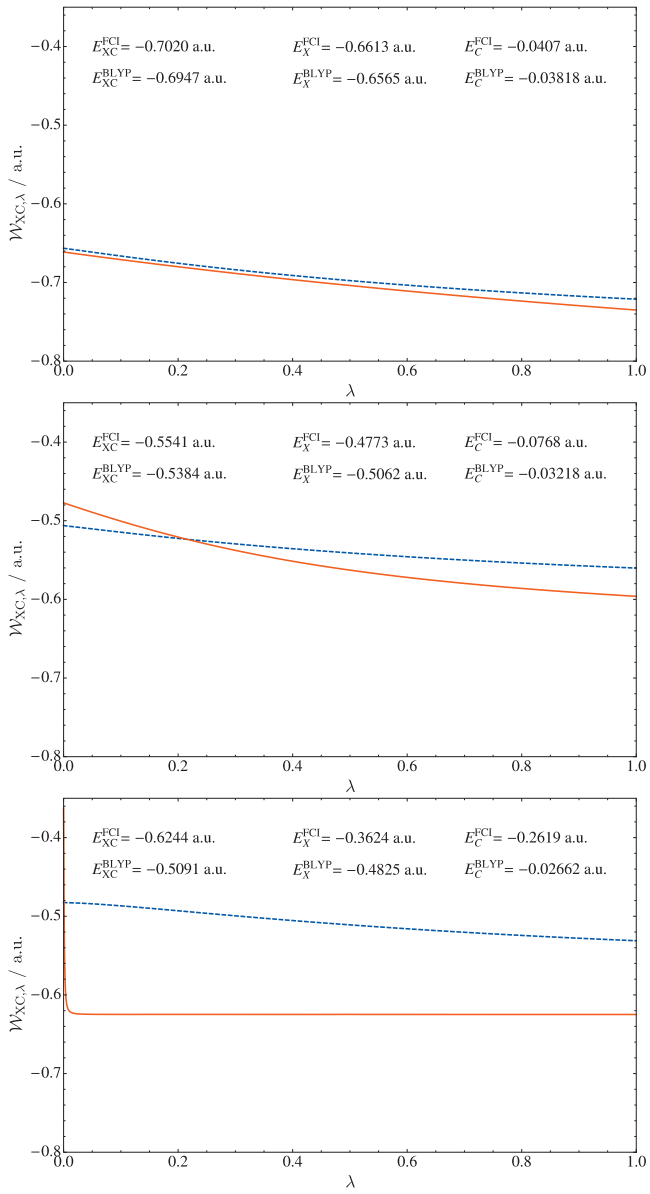

FIG. 10. The xc AC curves for the BLYP xc functional (dashed blue curves) compared with accurate curves (solid red) for the H_2 molecule at bond distances of 1.4 bohr (top), 3.0 bohr (middle), and 10.0 bohr (bottom).

also used by Ernzerhof[6] for the purpose of modeling the AC for the change in xc energy upon atomization.

The MCY AC integrands were presented in earlier work by one of us on the H_2 molecule and compared with the same AC model integrand, calculated using the exact slope and the exact fully interacting point, denoted as AC1.[19,20] As seen in that work, the MCY1 integrand has qualitatively the wrong behavior, having significant curvature at short bond lengths (where the exact curves are almost linear) and being linear at long bond lengths (where the exact curves exhibit their highest curvature). Since the AC1 model gives a reasonable reproduction of the accurate curves calculated here (although slightly underestimating the curvature at intermediate bond lengths), we will not reexamine this functional here, but rather focus on the BLYP functional, which is available in almost all quantum-chemistry codes supporting DFT.

In Fig. 10, we present the BLYP xc AC curves and the accurate FCI AC curves calculated here for the H_2 molecule at bond distances of 1.4, 3.0, and 10.0 bohr. These curves have been calculated for the self-consistent BLYP density; however, we have confirmed that evaluating them for the FCI density results in small, almost constant, shifts in the curves and does not lead to large changes in the energies obtained. In the top panel of Fig. 10, the curves at $R=1.4$ bohr (close to the equilibrium bond length) are presented. We see that BLYP provides a fairly faithful reproduction of the accurate AC curve, being slightly too high at all points along the curve, with a slightly larger error at the $\lambda=1$ end of the curve than at $\lambda=0$. The corresponding xc, exchange, and correlation energies are all slightly above the accurate values in this basis set.

In the middle panel of Fig. 10, we present the AC curves as the molecule is stretched to $R=3.0$ bohr. The curvature of the accurate AC curve is now clearly more pronounced than for the BLYP curve. For both curves, the xc and exchange energies become less negative than at $R=1.4$ bohr. However, for the exchange and correlation components of the energy, the BLYP functional under- and overestimates by −28.9 and 44.6 mH, respectively, leading to an overall xc error of just 15.7 mH. This behavior is clear from the crossing of the curves at $\lambda\approx0.22$. Indeed, this error cancellation steadily evolves, such that as the bond is stretched we can find areas on the potential energy surface where the total energy appears to be reasonably accurate, although in fact significant error cancellations are occurring.

Finally, in the bottom panel of Fig. 10, we present AC curves at $R=10.0$ bohr. The BLYP xc functional now overestimates the accurate value by as much as 18.5%. Significantly, this large BLYP error arises from a large but incomplete cancellation of the correlation overestimation by 235.3 mH (90%) and exchange underestimation by −120.1 mH (33%). In fact, we note that the LYP correlation energy actually becomes more positive as the bond is stretched, whereas the FCI correlation value becomes more negative (to recover static correlation). This qualitative BLYP failure is clear from the shapes of the xc AC curves in Fig. 10, which are determined by the correlation contribution since removal of the exchange simply corresponds to shifting the curve by a constant. We note that the calculations of the present work are performed in a restricted formalism, while the B88X and LYP functionals are derived for spin densities and may yield much improved results in unrestricted calculations. However, these functionals are in practice often applied in a restricted formalism. The calculation of the AC for unrestricted calculations is an area for future work.

Given the poor quality of the BLYP curves, we see that the strategy of making the MCY1 integrand intercept the BLYP curve at $\lambda=0.63$ is bound to be unsuccessful. This error could be offset, at least at intermediate bond lengths, by introducing a functional for the initial slope that overestimates the GL2 value in Eq. (36). However, in our experience, this value is typically underestimated by DFAs. Indeed, this observation probably explains the need to introduce a factor of 4.0 in front of $\mathcal{W}'_{xc,0}[\rho]$ in the definition of the MCY1 functional.[9] Combined, these observations highlight the need for an accurate method for calculating AC curves to

guide in the construction of approximate forms and avoid spurious error cancellations. The [1/1]–Padé form used in the MCY1 functional also illustrates the need for accurate input parameters, given a sufficiently flexible form. When evaluated using the exact exchange energy, the slope at $\lambda=0$ and the value at $\lambda=1$, this form can provide highly accurate AC curves. However, when approximate input parameters are used, this latent accuracy can remain hidden.

B. The ISI model

We now turn our attention to perhaps the most prominent and successful AC model based on relatively easily calculable input parameters—namely, the ISI model,[12,13,30,31] which represents an approximate resummation of the Görling–Levy perturbation series.[45,46] The ISI model uses approximate functionals derived using a polarization-plus-continuum (PC) model to describe the AC integrand in the strictly correlated ($\lambda=\infty$) limit,

$$\mathcal{W}_\lambda^{\mathrm{ISI}} = \mathcal{W}_\infty + \frac{X}{\sqrt{1+Y}+Z}, \tag{77}$$

where

$$X = \frac{xy^2}{z^2}, \quad Y = \frac{x^2y^2}{z^4}, \quad Z = \frac{xy^2}{z^3} - 1, \tag{78}$$

$$x = -2\mathcal{W}_0', \quad y = \mathcal{W}_\infty', \quad z = \mathcal{W}_0 - \mathcal{W}_\infty, \tag{79}$$

with

$$\mathcal{W}_{\mathrm{xc},\infty}^{\mathrm{PC}}[\rho] = \int \left[A\rho^{4/3}(\mathbf{r}) + B\frac{|\nabla\rho(\mathbf{r})|^2}{\rho^{4/3}(\mathbf{r})} \right] \mathrm{d}\mathbf{r}, \tag{80}$$

$$\mathcal{W}_{\mathrm{xc},\infty}'^{\mathrm{PC}}[\rho] = \int \left[C\rho^{3/2}(\mathbf{r}) + D\frac{|\nabla\rho(\mathbf{r})|^2}{\rho^{7/6}(\mathbf{r})} \right] \mathrm{d}\mathbf{r}, \tag{81}$$

which represent the coefficients in the asymptotic expansion

$$\mathcal{W}_\lambda[\rho] \to \mathcal{W}_\infty[\rho] + \mathcal{W}_\infty'[\rho]\lambda^{-1/2} + \mathcal{O}(\lambda^{-n/2}). \tag{82}$$

We note that the AC forms, Eqs. (55) and (72), developed in the present work also give a finite value $\mathcal{W}_\lambda[\rho]$ in the strictly correlated limit but that they depend asymptotically on λ^{-2} rather than on $\lambda^{-1/2}$, the latter dependence arising from zero-point oscillations of the system at large λ around its strictly correlated state,[12,56] unaccounted for in our models.

The two functionals in Eqs. (80) and (81) depend on the four constants A, B, C, and D. For the first three constants, we use $A=-(9/10)(4\pi/3)^{1/3}$, $B=(3/350)(3/4\pi)^{1/3}$, and $C=\frac{1}{2}(3\pi)^{1/2}$ from Ref. 12. For the last constant D, we explore the three options D_0, D_1, and D_2 proposed in Ref. 12 and a recently proposed value D_3 from Ref. 56. The constant $D_0=\frac{1}{40}(3/4\pi)^{1/6}$ derived from the PC model is positive; however, in Ref. 12, it was noted that this term should be negative to ensure that the functional of Eq. (81) gives the correct value of zero for one-electron densities. As such, two other parameters were proposed: $D_1=-0.030\,676$, obtained by ensuring that $\mathcal{W}_{\mathrm{xc},\infty}'[\rho]$ is zero for any exponential (hydrogenic) one-electron spherical density, and $D_2=-0.025\,58$, chosen so that the value of the functional above agrees with the corresponding expression for the meta-GGA of Ref. 57 on the two-electron density of the helium atom. The parameter $D_3=-0.028\,957$ was determined in a similar fashion to the D_1 parameter, instead ensuring that the functional gives the correct strictly correlated limit for the helium atom, see Ref. 56 for further details.

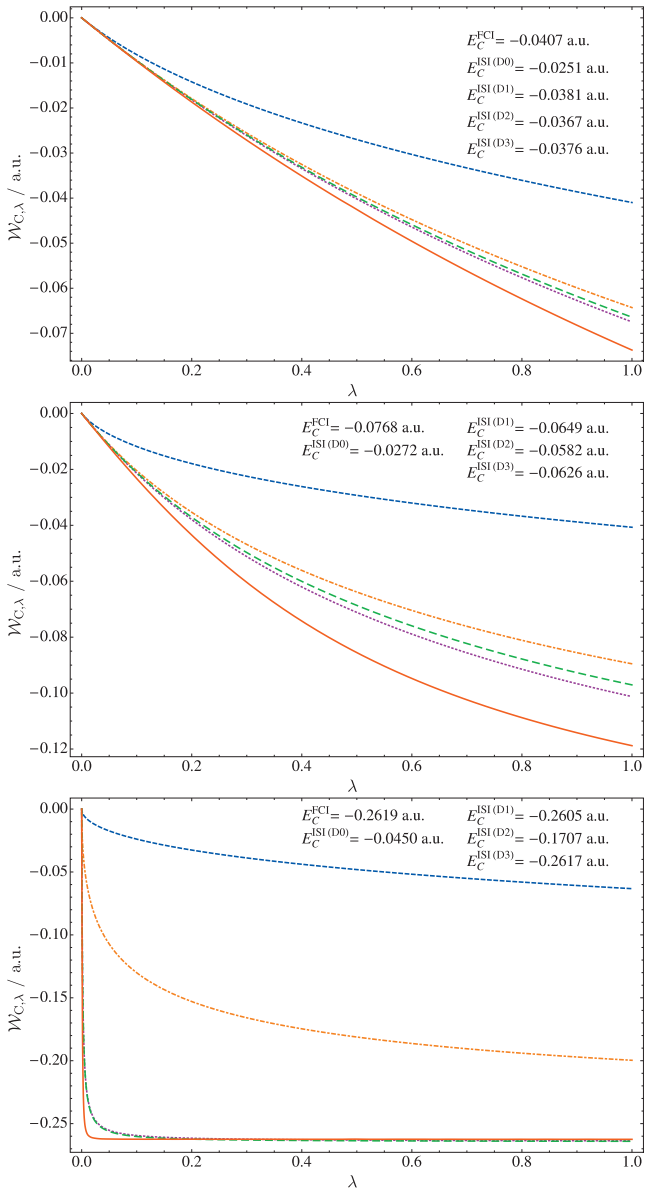

FIG. 11. AC correlation curves for the ISI xc functional compared with the accurate (solid red) curves for the H_2 molecule at bond distances of 1.4 bohr (top), 3.0 bohr (middle), and 10.0 bohr (bottom). Four definitions of the parameters are considered labeled D_0 (dashed blue curves), D_1 (dotted purple curves), D_2 (dot-dashed orange curves), and D_3 (long-dashed green curves), see text and Refs. 12 and 56 for details.

In Fig. 11, we compare the FCI AC integrand with the ISI model integrands for correlation (the above xc expression minus the KS exchange energy) calculated for the FCI density of H_2 at bond distances of 1.4, 3.0, and 10.0 bohr using the three different parameters D_0, D_1, and D_2 in the definition of $\mathcal{W}_{\mathrm{xc},\infty}'^{\mathrm{PC}}[\rho]$. The first point to note is that unlike the BLYP functional, the ISI model uses a full complement of orbital-dependent exchange and so there are no error cancellations between this and the correlation component, as ob-

served for the BLYP functional. In addition, the ISI model utilizes the exact slope at $\lambda=0$, the effect of which is clearly evident at all bond lengths.

The three ISI curves shown on each plot in Fig. 11 share the same $\mathcal{W}^{\mathrm{PC}}_{\mathrm{xc},\infty}[\rho]$ value but their accuracy is critically dependent on the choice of the parameter D in $\mathcal{W}'^{\mathrm{PC}}_{\mathrm{xc},\infty}[\rho]$. At all bond lengths, D_1 is the most accurate, closely followed by D_3; D_0 is the poorest with D_2 intermediate. Clearly, the qualitative behavior of the ISI model is far superior to the BLYP functional in Fig. 10. The correlation energy, in particular, increases with increasing bond length, as does the curvature of the plot, in contrast to the behavior of the BLYP curves. However, it is important to bear in mind that this has been achieved at substantially higher cost due to the use of the exact slope which is twice the GL2 correlation energy.

The present calculations illustrate the critical importance of $\mathcal{W}'^{\mathrm{PC}}_{\mathrm{xc},\infty}[\rho]$ to the success of the ISI method. We note that the performance of the most accurate D_1-parametrized ISI functional at long bond lengths is probably biased toward this particular system, since this value of the parameter was derived for hydrogenic densities. However, it is noteworthy that the D_3-parametrized ISI functional, based on the strictly correlated limit of the helium atom,[56] also shows promising performance at all bond lengths. For the previously recommended D_2 parameter, the value of the xc energy is -533.1 mH, compared with the BLYP value of -509.1 mH. The results of Ref. 56 and the present work indicate that reparametrization of the ISI model could lead to substantial improvements.

Also presented in Ref. 56 was a revised-ISI (revISI) model, which removes a spurious λ^{-1} term in the asymptotic expansion of the ISI model. We have performed a similar analysis for this functional (not presented here), indicating that the quality obtained using the D_3-parametrized revISI model is of similar high quality to the ISI model for the short bond lengths, with similar performance at intermediate bond lengths and a modest improvement at the two longest bond lengths, being close to the D_1-parametrized ISI values.

C. Utilizing the PC model in the new models

We now explore the effect of utilizing the PC model for $\mathcal{W}^{\mathrm{PC}}_{\mathrm{c},\infty}[\rho]=\mathcal{W}^{\mathrm{PC}}_{\mathrm{xc},\infty}[\rho]-\mathcal{W}_{\mathrm{xc},0}[\rho]$ in the AC-D and AC-CI models of the present work. To this end, we utilize the functional of Eq. (80) to determine $\mathcal{W}^{\mathrm{PC}}_{\mathrm{c},\infty}[\rho]$, which is the asymptotic parameter a in the forms of Eqs. (55) and (72). The resulting expressions for the correlation energy [i.e., Eqs. (59) and (75) with $\lambda=1$] depend only on the initial slope (twice the GL2 correlation energy) and on the correlation component of the density functional of Eq. (80). As such, they represent practically applicable correlation functionals suitable for addition to a full complement of orbital-dependent exchange without cancellation of errors. The use of an approximate density functional for $\mathcal{W}_{\mathrm{c},\infty}[\rho]=a$ in the AC-D and AC-CI models will, of course, impact upon the accuracy obtained from these forms. To examine this effect, we compare in Fig. 12 the correlation AC curves for H_2 calculated from these forms with the exact AC curves.

In the upper panel of Fig. 12, the $\mathcal{W}_{\mathrm{AC\text{-}D}}[\rho]$ model, parametrized as described above, is compared with the corresponding exact FCI curve. Clearly, a degree of error cancellation occurs for all bond lengths greater than 1.4 bohr, as the curves cross the exact ones. Nevertheless, the correlation energy remains below the true values at all distances: by 1 mH (3%) at the two shortest bond lengths, 0.9 mH (1.2%) at 3 bohr, 3 mH at 5 and 7 bohr (1.6% and 1.4%, respectively), and by 2 mH (0.7%) at 10 bohr. These values constitute a substantial improvement over any of the ISI values shown in Fig. 11.

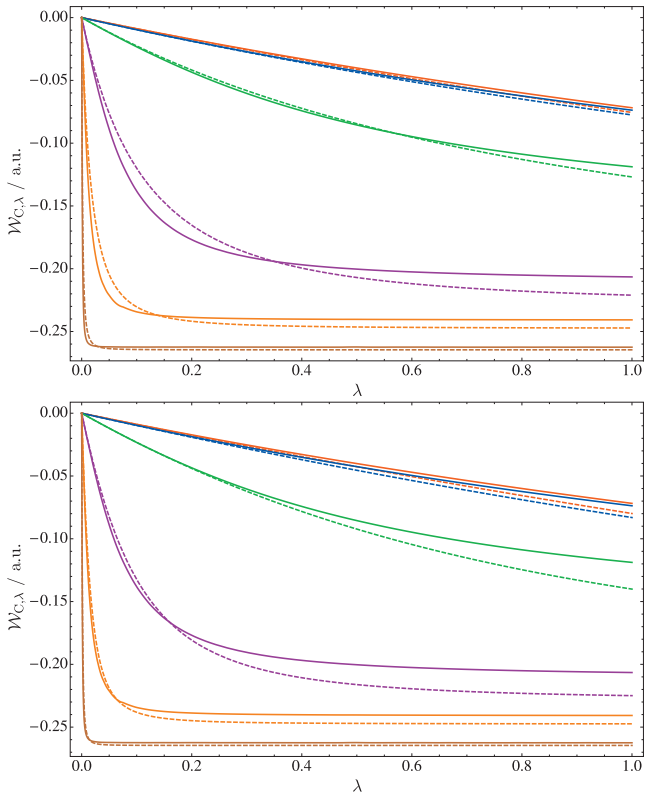

FIG. 12. Models in the present work evaluated using the $\mathcal{W}^{\mathrm{PC}}_{\mathrm{C},\infty}$ values, the AC-D model in part (a) and the AC-CI model in part (b).

In the lower panel of Fig. 12, we compare $\mathcal{W}_{\mathrm{AC\text{-}CI}}[\rho]$, parametrized as $\mathcal{W}_{\mathrm{AC\text{-}D}}[\rho]$ in the upper panel, with the FCI curve. For this CI form, error cancellations play a role for the longest three bond lengths but to a much lesser extent than for the AC-D model. At all bond lengths, the correlation energies are underestimated, this time by a more significant margin. For the shortest two bond lengths, the correlation energy is underestimated by 3 mH (8%), rising to 8 mH (10%) at 3 bohr. At 5 bohr, the error is 11 mH (6%); stretching the bond further, the errors decrease to 6 mH at 7 bohr (2.3%) and 2 mH (0.8%) at 10 bohr. Again, while less accurate than the similarly parametrized AC-D model, the AC-CI model provides a substantial improvement over the ISI model. Moreover, any improvements in the DFT description of the strongly interacting system will also reduce the error in the AC-CI model, unlike for the AC-D model.

Of course, as with all prospective xc functionals, the ultimate accuracy of these models must be assessed by careful benchmarking of a range of molecular properties over a large set of molecules, although these initial results show

promise. We note that a key ingredient of these functionals is the slope $\mathcal{W}_0'[\rho]$, which imparts a greater cost to these functionals than for standard functionals and an N^5 scaling with system size. On the other hand, these models do not suffer a divergence of the correlation energy as the bond in H_2 is stretched (as would be observed for second-order perturbation theories based on the KS determinant), the divergence instead being essential to describe the initial slope of the AC curve accurately.

For the above reasons, it is highly desirable to determine functionals for modeling $\mathcal{W}_0'[\rho]$ at reduced cost. To extract such a functional from existing xc functionals, we can employ the λ derivative of the scaling relation in Eq. (76). However, in our experience, such forms tend to underestimate strongly the slope as the bond is stretched. The development of new functionals specifically tailored to this task is therefore an area for future work with the aim to reduce the scaling of the functional with system size to the same level as in typical "hybrid" xc functionals.

V. CONCLUSIONS

In this work, we have outlined an approach for the rational design of xc and correlation functionals in DFT guided by our recent implementation of an approach for the calculation of accurate AC curves using wave-function techniques and the Lieb variation principle.[32,33] The systematic nature of the wave-function methods means that we may refine the calculated AC curves in a controlled manner to give an accurate description of the AC integrand at a range of electronic interaction strengths, and hence xc and correlation energies of DFT. By modeling the AC integrand, new forms for the xc energy can be constructed. The calculation of accurate AC curves affords us the opportunity to understand how well our models perform for the first time in both atomic and molecular systems. To approach the problem of constructing new functionals in a rational manner, we have considered a variety of wave-function methodologies, focusing on how their correlation energies vary with the interaction strength. We have constructed simple models designed to capture the physics of these variations and evaluated their interaction-strength derivatives leading to new simple parametrized models for AC curves.

We commenced by highlighting the small correlation energy contained in the HF model when viewed in the context of DFT. This small perturbation is well described by GL2 theory restricted to a single-determinant wave function. The resulting AC curves are then very close to linear, the correlation arising as a result of replacing the multiplicative KS exchange potential with a nonmultiplicative HF operator. As a result, the orbital energies vary in a linear fashion along the AC path such that the occupied-virtual energy differences increase.

We then showed that the description of dynamic correlation could be achieved using MP2 or CCSD methods. Considering the interaction-strength dependence of the MP2 correlation energy, a simple model for the AC curve, AC-D, was developed that shows superb accuracy for systems dominated by dynamic correlation. Similar considerations for the triples correction in CCSD(T) theory led to an AC model, AC-T, for the triples correction to the energy, which was itself well modeled by its lowest-order quadratic contribution.

To examine the effect of static correlation, we developed a simple minimal-basis CI model for the prototypical H_2 molecule. The high accuracy of this AC-CI model was demonstrated both by least-squares fitting of the parameters and by parametrization in terms of the initial slope and the fully interacting end point. Remarkably, the AC-D model also showed reasonable accuracy for H_2, although it was notably less accurate than the AC-CI model at intermediate bond lengths.

To emphasize the utility of accurate information on the AC integrand, we then analyzed the failure of the BLYP xc functional to describe bond dissociation in H_2 in a restricted formalism. At short bond lengths, the xc AC BLYP curve was shown to behave in a reasonable manner. However, as the bond was stretched, a cancellation of errors between a too negative exchange contribution and a too positive correlation contribution was observed. The ISI-model AC integrand was also examined and compared with FCI results, highlighting a strong sensitivity to the choice of parameters used in the functional for the asymptotic expansion coefficient $\mathcal{W}'^{\mathrm{PC}}_{\mathrm{xc},\infty}[\rho]$.

Finally, we reparametrized our new models in terms of the PC-model asymptotic value of the AC used in the ISI model. The PC value appears to be reasonably accurate for such a simple functional form and its inclusion in both the AC-D and AC-CI models leads to remarkably accurate and balanced models over a range of molecular bond lengths, compared with previous attempts. Work to assess the utility of PC value in modeling ACs for the dissociation of more complicated molecules is currently underway. Most importantly, these forms represent a family of correlation functionals that can be practically used as they do not involve recourse to the complicated interacting many-electron wave function. Indeed, future work will involve the self-consistent implementation of these forms and the development of lower-cost functionals for modeling the initial slope of the AC curve. To ensure that spurious error cancellations do not enter these new forms, the calculation of accurate ACs will continue to play a central role.

ACKNOWLEDGMENTS

The authors thank A. Savin and P. Gori-Giorgi for useful discussions and drawing their attention to improved ISI models of Ref. 56. This work has been supported by the CoE Centre for Theoretical and Computational Chemistry through Grant No. 179568/V30. A.M.T. gratefully acknowledges support from the Norwegian Research Council through Grant No. 171185.

[1] J. Harris and R. O. Jones, J. Phys. F: Met. Phys. **4**, 1170 (1974).
[2] D. C. Langreth and J. P. Perdew, Solid State Commun. **17**, 1425 (1975).
[3] O. Gunnarsson and B. I. Lundqvist, Phys. Rev. B **13**, 4274 (1976).
[4] O. Gunnarsson and B. I. Lundqvist, Phys. Rev. B **15**, 6006 (1977).
[5] D. C. Langreth and J. P. Perdew, Phys. Rev. B **15**, 2884 (1977).
[6] M. Ernzerhof, Chem. Phys. Lett. **263**, 499 (1996).
[7] M. Ernzerhof, J. P. Perdew, and K. Burke, Int. J. Quantum Chem. **64**,

285 (1997).
[8] M. Fuchs, Y. Niquet, X. Gonze, and K. Burke, J. Chem. Phys. **122**, 094116 (2005).
[9] P. Mori-Sánchez, A. J. Cohen, and W. Yang, J. Chem. Phys. **124**, 091102 (2006).
[10] A. J. Cohen, P. Mori-Sánchez, and W. Yang, J. Chem. Phys. **127**, 034101 (2007).
[11] K. Burke, M. Ernzerhof, and J. P. Perdew, Chem. Phys. Lett. **265**, 115 (1997).
[12] M. Seidl, J. P. Perdew, and S. Kurth, Phys. Rev. A **62**, 012502 (2000).
[13] M. Seidl, Int. J. Quantum Chem. **91**, 145 (2002).
[14] D. P. Joubert and G. P. Srivastava, J. Chem. Phys. **109**, 5212 (1998).
[15] F. Colonna and A. Savin, J. Chem. Phys. **110**, 2828 (1999).
[16] D. Frydel, W. M. Terilla, and K. Burke, J. Chem. Phys. **112**, 5292 (2000).
[17] A. Savin, F. Colonna, and M. Allavena, J. Chem. Phys. **115**, 6827 (2001).
[18] R. Pollet, F. Colonna, T. Leininger, H. Stoll, H.-J. Werner, and A. Savin, Int. J. Quantum Chem. **91**, 84 (2002).
[19] M. J. G. Peach, A. M. Teale, and D. J. Tozer, J. Chem. Phys. **126**, 244104 (2007).
[20] M. J. G. Peach, A. M. Miller, A. M. Teale, and D. J. Tozer, J. Chem. Phys. **129**, 064105 (2008).
[21] W. Yang, J. Chem. Phys. **109**, 10107 (1998).
[22] A. M. Teale, S. Coriani, and T. Helgaker, "Range-dependent adiabatic connections," AIP Conf. Proc. (to be published).
[23] A. D. Becke, J. Chem. Phys. **98**, 1372 (1993).
[24] A. D. Becke, Phys. Rev. A **38**, 3098 (1988).
[25] C. Lee, W. Yang, and R. G. Parr, Phys. Rev. B **37**, 785 (1988).
[26] A. D. Becke, J. Chem. Phys. **98**, 5648 (1993).
[27] S. H. Vosko, L. Wilk, and M. Nusair, Can. J. Phys. **58**, 1200 (1980).
[28] P. J. Stephens, F. J. Devlin, C. F. Chabalowski, and M. J. Frisch, J. Phys. Chem. **98**, 11623 (1994).
[29] J. Perdew, M. Emzerhof, and K. Burke, J. Chem. Phys. **105**, 9982 (1996).
[30] M. Seidl, J. P. Perdew, and M. Levy, Phys. Rev. A **59**, 51 (1999).
[31] M. Seidl, J. P. Perdew, and S. Kurth, Phys. Rev. Lett. **84**, 5070 (2000).
[32] Q. Wu and W. Yang, J. Chem. Phys. **118**, 2498 (2003).
[33] A. M. Teale, S. Coriani, and T. Helgaker, J. Chem. Phys. **130**, 104111 (2009).
[34] E. Lieb, Int. J. Quantum Chem. **24**, 243 (1983).
[35] W. Yang and Q. Wu, Phys. Rev. Lett. **89**, 143002 (2002).
[36] E. Fermi and E. Amaldi, Mem. Accad. Italia **6**, 117 (1934), reproduced in "Collected Papers (Note e Memorie)," loc. cit, as art No. 82. For further information reprint is available at http://www.archive.org/stream/collected papersn007155mbp#page/n19/mode/2up.
[37] T. H. Dunning, J. Chem. Phys. **90**, 1007 (1989).
[38] R. A. Kendall, T. H. Dunning, and R. J. Harrison, J. Chem. Phys. **96**, 6796 (1992).
[39] D. E. Woon and T. H. Dunning, J. Chem. Phys. **100**, 2975 (1994).
[40] D. E. Woon and T. H. Dunning, J. Chem. Phys. **103**, 4572 (1995).
[41] DALTON, a molecular electronic structure program, release 2.0, 2005, see http://www.kjemi.uio.no/software/dalton/dalton.html.
[42] T. Helgaker, P. Jørgensen, and J. Olsen, *Modern Electronic-Structure Theory* (Wiley, New York, 2000).
[43] T. Helgaker and P. Jørgensen, Theor. Chim. Acta **75**, 111 (1989).
[44] T. Helgaker and P. Jørgensen, in *Methods in Computational Molecular Physics*, edited by S. Wilson and G. H. F. Diercksen (Plenum, New York, 1992), p. 353.
[45] A. Görling and M. Levy, Phys. Rev. B **47**, 13105 (1993).
[46] A. Görling and M. Levy, Phys. Rev. A **50**, 196 (1994).
[47] A. Görling and M. Ernzerhof, Phys. Rev. A **51**, 4501 (1995).
[48] T. Helgaker, W. Klopper, H. Koch, and J. Noga, J. Chem. Phys. **106**, 9639 (1997).
[49] A. Halkier, T. Helgaker, P. Jørgensen, W. Klopper, H. Koch, J. Olsen, and A. K. Wilson, Chem. Phys. Lett. **286**, 243 (1998).
[50] MATHEMATICA, Version 7.0.0, Wolfram Research, Inc., Champaign, Illinois, 2009.
[51] J. P. Perdew, E. R. McMullen, and A. Zunger, Phys. Rev. A **23**, 2785 (1981).
[52] W. Yang, in *Density Matrices and Density-Functionals*, edited by R. Erdahl and V. H. Smith, Jr. (Reidel, Dordrecht, Holland, 1987), p. 499.
[53] M. Levy and J. P. Perdew, in *Single-Particle Density in Physics and Chemistry*, edited by N. H. March and B. M. Deb (Academic, New York, 1987), pp. 54–55.
[54] M. Levy and J. Perdew, Phys. Rev. A **32**, 2010 (1985).
[55] J. M. Tao, J. P. Perdew, V. N. Staroverov, and G. E. Scuseria, Phys. Rev. Lett. **91**, 146401 (2003).
[56] P. Gori-Giorgi, G. Vignale, and M. Seidl, J. Chem. Theory Comput. **5**, 743 (2009).
[57] J. P. Perdew, S. Kurth, A. Zupan, and P. Blaha, Phys. Rev. Lett. **82**, 2544 (1999).